Origin and distribution of grain-coating and pore-filling chlorite in deltaic sandstones for reservoir quality assessment

Griffiths, Joshua ; Worden, Richard H. ; Utley, James E.P. ; Brostrøm, Christian ; Martinius, Allard W.; Lawan, Auwalu Y. ; Al-Hajri, Ali I.

DOI
10.1016/j.marpetgeo.2021.105326

Publication date
2021

Document Version
Final published version

Published in
Marine and Petroleum Geology

Citation (APA)
Griffiths, J., Worden, R. H., Utley, J. E. P., Brostrøm, C., Martinius, A. W., Lawan, A. Y., & Al-Hajri, A. I. (2021). Origin and distribution of grain-coating and pore-filling chlorite in deltaic sandstones for reservoir quality assessment. *Marine and Petroleum Geology*, *134*, 1-23. Article 105326. https://doi.org/10.1016/j.marpetgeo.2021.105326

Marine and Petroleum Geology 134 (2021) 105326

Contents lists available at ScienceDirect

Marine and Petroleum Geology

journal homepage: www.elsevier.com/locate/marpetgeo

Origin and distribution of grain-coating and pore-filling chlorite in deltaic sandstones for reservoir quality assessment

Joshua Griffiths [a,b], Richard H. Worden [a,*], James E.P. Utley [a], Christian Brostrøm [c], Allard W. Martinius [c,d], Auwalu Y. Lawan [a,e], Ali I. Al-Hajri [a]

[a] Department of Earth, Ocean and Ecological Sciences, University of Liverpool, Liverpool, UK
[b] BP Renewal, Sunbury-on-Thames, Middlesex, UK
[c] Equinor ASA, Arkitekt Ebbells veg 10, N-7053, Ranheim, Norway
[d] Technical University of Delft, Stevinweg 1, 2628 CN, Delft, Netherlands
[e] Department of Geology, Bayero University, Kano, Nigeria

ARTICLE INFO

Keywords:
Chlorite
Grain-coating chlorite
Pore-filling chlorite
Deltaic sandstones
Reservoir quality
SEM-EDS
Porosity
Permeability

ABSTRACT

Grain-coating chlorite preserves porosity and permeability through the inhibition of quartz cement whereas pore-filling chlorite blocks pore-throats and diminishes reservoir quality. The aim of this study is to determine the origin and principal mechanisms which govern the distribution of grain-coating and pore-filling chlorite in Jurassic deltaic sandstones (Tilje Formation, Smørbukk field, Mid Norwegian Shelf). The study focussed on very high-density sampling for petrographic analysis, from three sections of sandstone core from the same well with contrasting reservoir quality, rather than the low-density sampling approach typically employed. The aim was to gain new understanding of specific controls on porosity and permeability based on core description, core analysis measurements and a suite of petrographic techniques. Results of this study show grain-coating chlorite originated from the thermally-driven recrystallisation of detrital clay coats and/or clay mineral precursors. Pore-filling chlorite has principally derived from the ductile deformation of chlorite-rich Fe-ooids, that were possibly reworked from a proximal evaporitic setting. The distribution of chlorite precursor material, detrital clay coats, and subsequently the distribution of grain-coating and pore-filling chlorite, were controlled by the relative dominance of tidal and fluvial processes active during sediment deposition. Optimum grain-coating chlorite is found in tidal-fluvial sandstones with moderate fluvial influence. Pore-filling chlorite is pervasive in tidal-fluvial channel sandstones deposited during periods of high fluvial discharge, or proximal to the central turbidity maximum zone; marked by an abundance of fluid mud. Tidal channel sandstones with no fluvial influence are pervasively quartz cemented due to an absence of grain-coating chlorite. Grain-coating chlorite and good reservoir quality occurs in heterolithic distributary mouth bar sandstones, however mixing of mud- and sand-prone facies due to intense bioturbation has reduced permeability. Results from this study can be used to predict reservoir quality in the Smørbukk field and in analogous shallow-marine sandstones worldwide.

1. Introduction

Reservoir quality is quantified through the measurement of porosity, which controls the volume of oil or gas in place, and permeability, which controls the rate at which oil or gas flow from the reservoir to the wellbore (Gluyas and Swarbrick, 2004). Porosity and permeability (reservoir quality), and thus economic viability of quartzose sandstone reservoirs, typically reduce with increasing burial depth and prolonged thermal-exposure primarily due to compaction and quartz cementation (Lander et al., 2008; Ramm, 1992; Worden and Burley, 2003). Paradoxically, in the search for cost-competitive 'advantaged oil and gas', operators are targeting high-temperature and deeply buried reservoirs in the quest for high permeability reservoirs that can be produced at an economic rate. One possible mechanism of preserving exceptionally high-porosity and permeability in Mesozoic (and older), and even some Palaeogene, deeply buried and thermally stressed sandstones (>2.5–3 km; > 80–100 °C) is the inhibition of quartz cementation. Quartz cement may be retarded due to a number of factors, such as chlorite- (Ehrenberg,

* Corresponding author.
E-mail address: r.worden@liv.ac.uk (R.H. Worden).

https://doi.org/10.1016/j.marpetgeo.2021.105326
Received 15 January 2021; Received in revised form 4 August 2021; Accepted 7 September 2021
Available online 9 September 2021

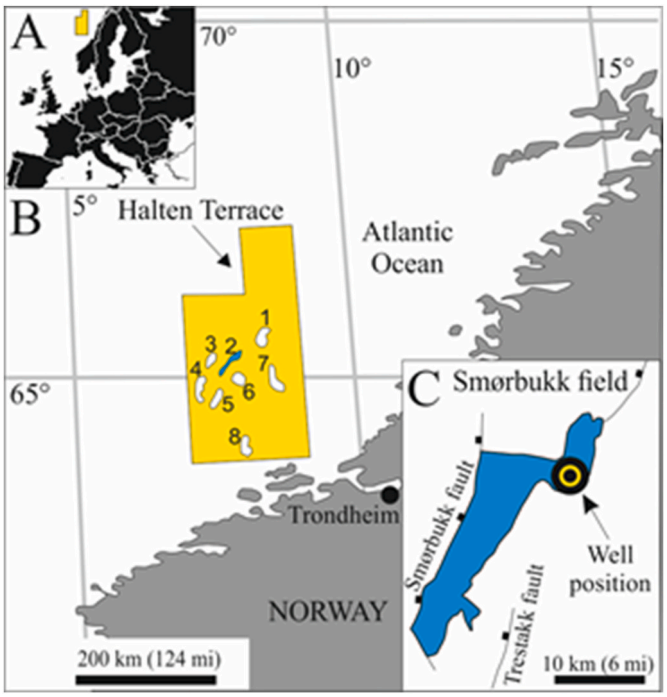

Fig. 1. Location of the Smørbukk field, offshore Norway, modified after Ichaso and Dalrymple (2014). (A) Position of the Halten Terrace area (yellow). (B) Position of hydrocarbon fields in the Halten terrace area: (1) – Heidrun, (2) Smørbukk (Åsgard; blue), (3) Morvin, (4) Kristin, (5) Lavrans, (6) Smørbukk Sør (Åsgard), and (8) Njord. (C) Map of the Smørbukk field with approximate position of well 6506/12-N-4 used in this study (yellow & black rings). (For interpretation of the references to colour in this figure legend, the reader is referred to the Web version of this article.)

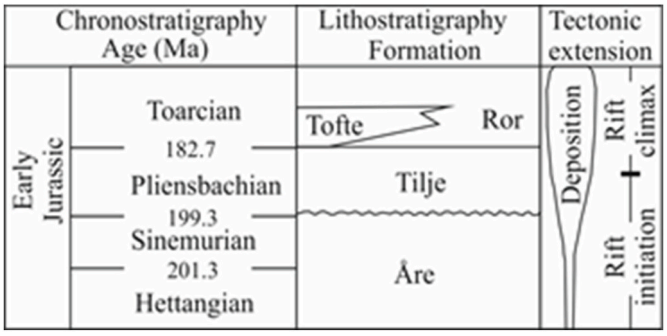

Fig. 2. Stratigraphic context of the Early Jurassic Tilje Formation (this study) and associated tectonic extension, modified after Ichaso et al. (2016).

1993), microcrystalline quartz- (Aase et al., 1996), and siderite- (Karim et al., 2010) grain coats, and, under some circumstances, early oil-emplacement (Worden et al., 2018b). The focus of this study is understanding the origin and distribution of authigenic grain-coating chlorite (Ehrenberg, 1993; Stricker and Jones, 2016; Worden et al., 2020). Chlorite grain coats are important since individual chlorite flakes, in clay coats, preserve porosity by acting as barriers to the lateral coalescence of epitaxial micro-quartz cement and subsequent growth of pore-filling syntaxial quartz overgrowths (Ajdukiewicz and Larese, 2012; Billault et al., 2003; Bloch et al., 2002; Stricker and Jones, 2016; Zhu et al., 2017).

Despite being over 60 years since grain-coating chlorite was discovered to preserve high-porosity in deeply-buried sandstones (Heald and Anderegg, 1960; Pittman and Lumsden, 1968), the energy industry struggles to predict its occurrence and distribution. To complicate matters, chlorite may be pore-filling, for example, if chlorite grain-coats are too thick they can block pore throats and lower permeability, as observed in the Krechba field, Algeria (Armitage et al., 2010). In contrast, if chlorite grain-coats are too thin, or discontinuous, quartz cement will form between the gaps in the coat and degrade reservoir quality, as reported in the Petrel field, Australia (Saïag et al., 2016). In this study we refer to the optimum authigenic grain coat thickness and continuity as the 'chlorite Goldilocks zone' in which grain coats are neither too thin, or too thick, and instead are "just right", after "The story of the three bears" by Southey (1837), and first used by Wooldridge et al. (2017b) in the context of grain coats.

Authigenic chlorite grain-coats have been reported to originate from (i) clay precursor at shallow burial depth (<1000 m, < 40 °C) which have undergone thermally-driven recrystallisation (Beaufort et al., 2015; Virolle et al., 2021), and (ii) *in situ* growth from the authigenic alteration of precursor and early-diagenetic minerals, which interact with pore fluids during burial (Aagaard et al., 2000; Ajdukiewicz and Larese, 2012; Bloch et al., 2002; Hillier, 1994; Worden et al., 2020; Worden and Morad, 2003; Zhu et al., 2017). Clay precursors such as berthierine originate from detrital clay coats, which demonstrates the importance of depositional environment characterisation in understanding the occurrence of chlorite in sedimentary strata. As a result, recent modern analogue studies have been designed in order to establish how detrital clay coats and precursor minerals (detrital and early-diagenetic) are distributed in the primary depositional environment (Dowey et al., 2017; Griffiths et al., 2018, 2019a, 2019b; Virolle et al., 2019a, 2019b, 2020; Wooldridge et al., 2017a, 2017b, 2018). The aim of this study was to establish the origin and controls on the distribution of pore-filling and grain-coating chlorite in Jurassic deltaic sandstones based on the sedimentological and petrophysical characterisation of the Tilje Formation, Smørbukk field (Mid Norwegian Shelf, part of the Åsgard Unit; Fig. 1).

Based on an unusually high-density sampling strategy from a single well, three sandstone sections that have entirely contrasting reservoir quality, the specific objectives of this paper are to:

(1) establish primary depositional processes active during sediment deposition and so reconstruct palaeoenvironment conditions,
(2) determine the major controls on sandstone reservoir quality,
(3) determine the origin of grain-coating and pore-filling chlorite,
(4) determine the principal mechanisms which govern the distribution of grain-coating and pore-filling chlorite,

Addressing these objectives is needed to better understand the distribution of grain-coating and pore-filling chlorite on a play fairway scale in the Smørbukk field and to develop a prospect-scale understanding of the controls on reservoir quality to maximise ultimate recovery.

2. Smørbukk field (Tilje formation), Halten terrace, offshore Norway

The Halten Terrace (Fig. 1) is a 130 km by 80 km rhomboidal tectonic section of the Haltenbanken area. The Halten Terrace is a mature hydrocarbon province with offshore production principally derived from heterolithic Early and Middle Jurassic synrift siliciclastic shallow-marine sandstones deposited during the opening of the North Atlantic Ocean (Ichaso and Dalrymple, 2009, 2014; Ichaso et al., 2016; Martinius et al., 2001, 2005). Gas and condensate were sourced from the thermal maturation of coals of the Early Jurassic Åre Formation while oil was derived from the Late Jurassic Spekk Formation (Martinius et al., 2005) which charged two main reservoir groups (Båt and Fangst Groups). The Early Jurassic Tilje Formation forms part of Båt Group and is a significant reservoir interval in several large North Sea hydrocarbon fields, including the Smørbukk field (the focus of this study; Fig. 1B). Together Smørbukk, Smørbukk Sør and Midgard prospects form the Åsgard field

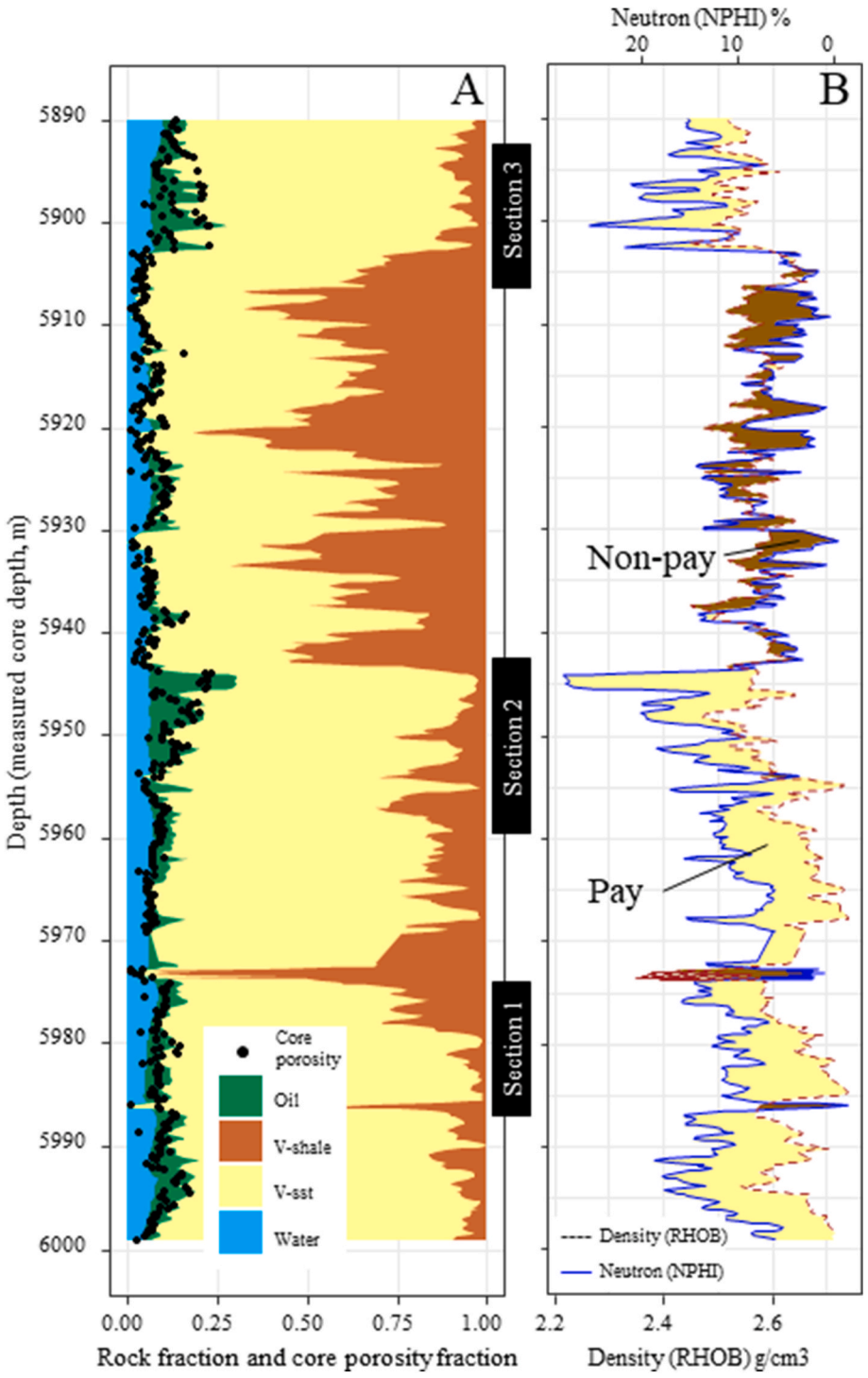

Fig. 3. Wireline logs and the locations of the three sections of core intensively analysed in this study. (A) Wireline-log derived lithology, with porosity calculated using the density log and the pore-fluids derived using the Archie equation and the deep resistivity log (Rider and Kennedy, 2011). The solid fraction of the rock was arbitrarily split between sandstone and "shale" by using a Vshale calculation (Rider and Kennedy, 2011) based on the gamma log. The Vshale calculation relies on clay minerals being dominated by radioactive illite, as opposed to non-radioactive chlorite, and so may not be wholly accurate in the context of the chlorite-rich clay mineral suite in the Tilje Fm. (B) A conventional neutron-density cross-over diagram with nominal pay (density to the left of the neutron value) and non-pay (density to the right of the neutron value). This diagram may not wholly reflect pay and non-pay in the Tilje Formation as these sandstones are relatively rich in chlorite which has a disproportionately high neutron response (Worden et al., 2020). The three sections of core are marked to the right of Fig. 3A with Section 1 represented in Fig. 5 containing facies association 1, Section 2 represented in Fig. 6 containing facies association 2, and Section 3 represented in Fig. 7 containing facies association 3.

(Klefstad et al., 2005).

The Smørbukk field was discovered in 1984 and is located 230 km west of the Norwegian mainland (Corfield and Sharp, 2000; Ehrenberg et al., 1992); it contains five reservoir intervals (Åre, Tilje, Ile, Tofte, and Garn Formations) (Martinius et al., 2005). Gas condensate and volatile oil (43–48 API°) are structurally trapped in a tilted fault block, with booked recoverable reserves totalling 57 $\times$ 10^6 standard m^3 (359 MMbbl) of oil and 91 $\times$ 10^9 standard m^3 of gas (3.2 tcf) (producing or sanctioned for development, as of 2003) (Martinius et al., 2005).

Several studies over the past three decades have focused on better understanding reservoir architecture of the 100–300 m thick, highly heterogeneous, Lower Jurassic Åre and Tilje Formations to aid hydrocarbon extraction (Dreyer, 1992; Ichaso and Dalrymple, 2009; Ichaso et al., 2016; Martinius et al., 2001, 2005). The Åre and Tilje successions represent synrift deposits that accumulated in the 130 km by 80 km north-northeast south-southwest orientated (Fig. 2), structurally controlled embayment that formed during the early phase of Jurassic rifting in the Halten area (Ichaso and Dalrymple, 2014; Marsh et al., 2010). Shallow-marine sedimentation patterns were strongly governed by tidal currents, with occasional significant river influence and minor wave action except at distal locations (Ichaso and Dalrymple, 2009, 2014; Ichaso et al., 2016; Martinius et al., 2001, 2005). In addition to

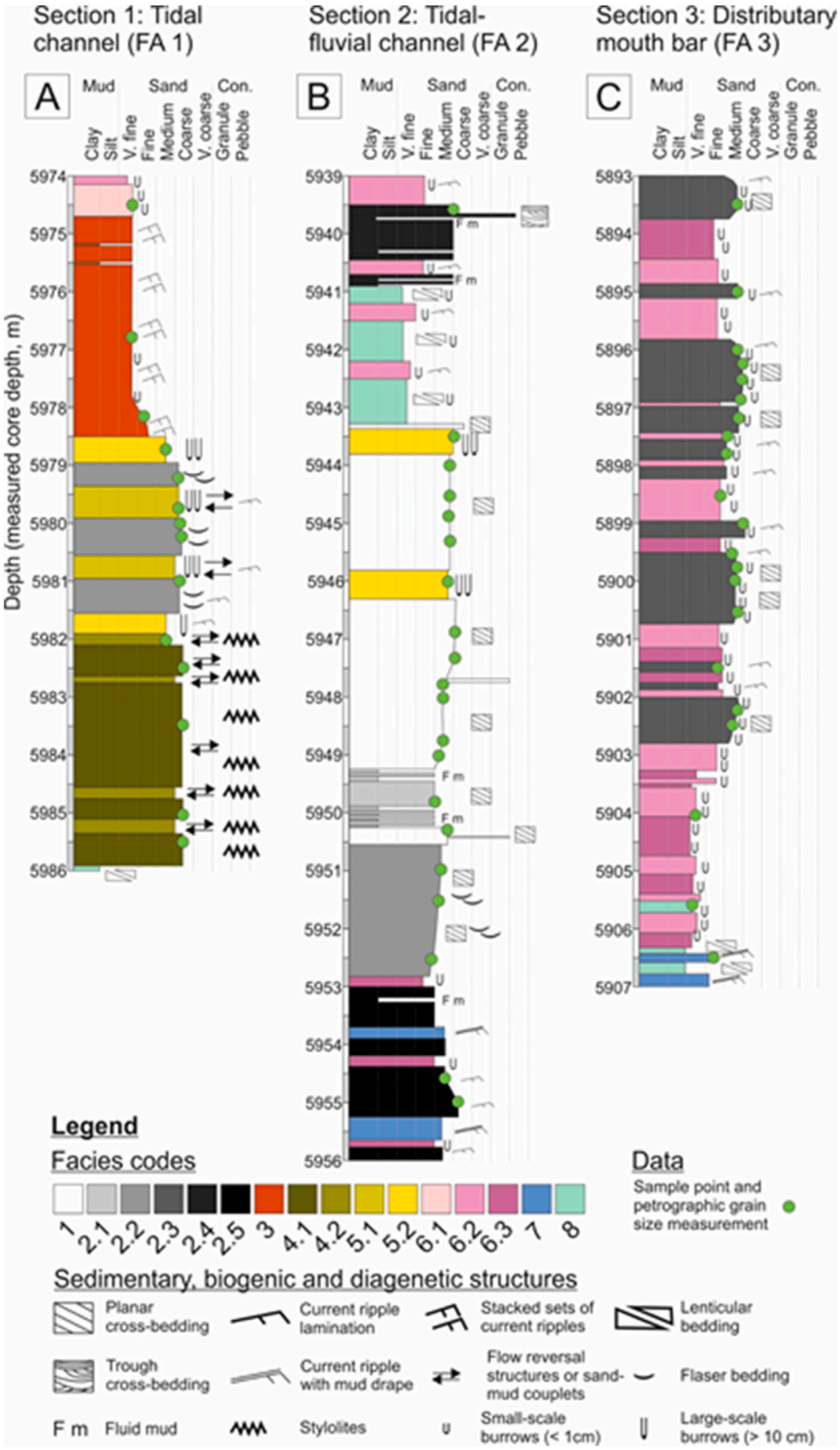

Fig. 4. Sedimentary logs through the three selected sections of sandstone-dominated core with interpreted facies scheme presented. The colour-scheme selected for the facies is the same as that used in boxplots in Figs. 8, 13 and 20. (For interpretation of the references to colour in this figure legend, the reader is referred to the Web version of this article.)

complex facies heterogeneity, the economic viability of the Tilje Formation in the Smørbukk field has been reported to be further controlled by the distribution and completeness of grain-coating chlorite, and thus quartz cementation (Ehrenberg, 1993).

3. Methods

Based on facies and reservoir quality (porosity and permeability) variability three Tilje Formation core intervals was chosen by the

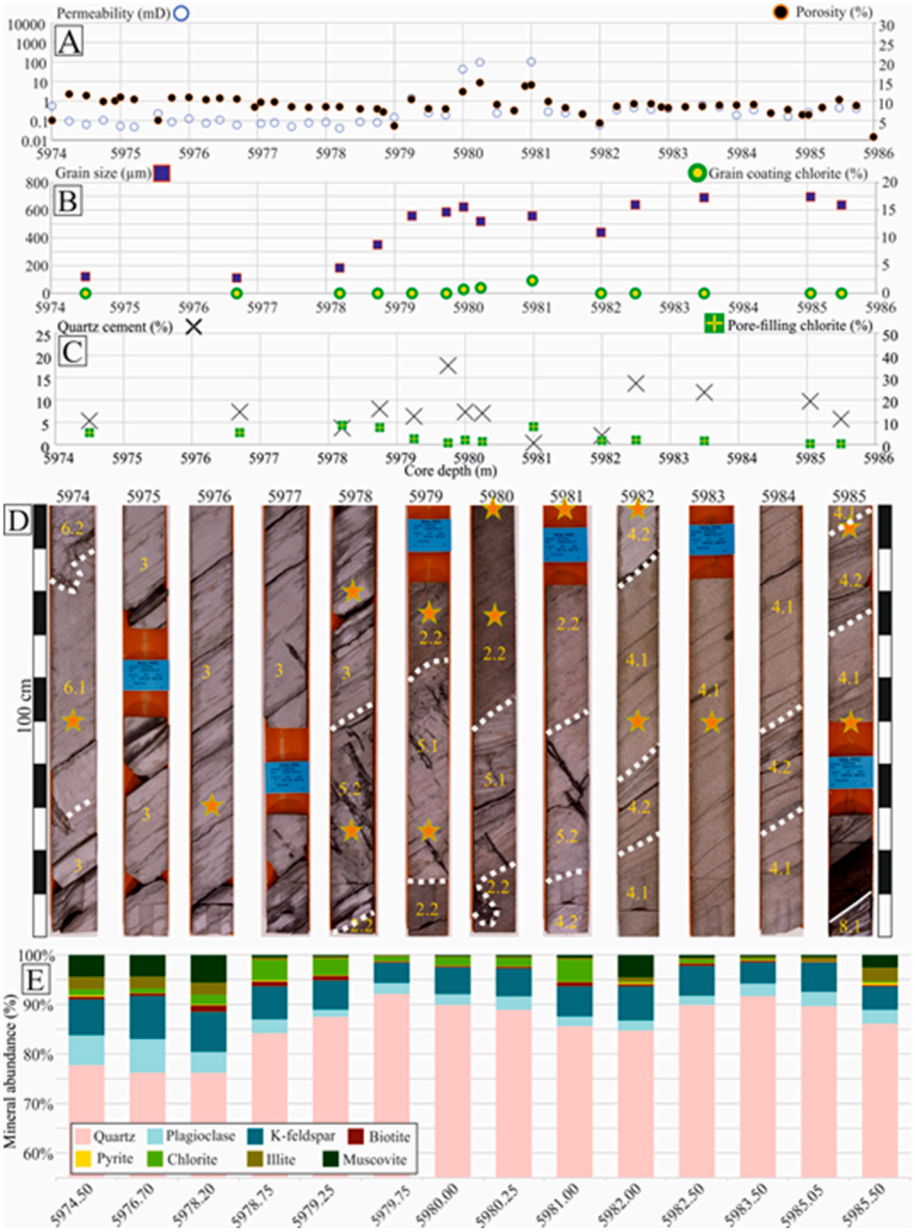

Fig. 5. Summary panel of section one (S1; base interval, Fig. 3) from 5986 to 5974 m (measured depth), interpreted to be deposited in a tidal-channel setting. Note that this core is wholly in facies association 1. (A) Porosity (%; dark brown circles with orange rim) and permeability (mD; hollow blue circles) versus depth. (B) Grain-coating chlorite (%; yellow circles with green rim) and grain size (average; blue square with red rim) versus depth. (C) Pore-filling chlorite (%; yellow cross in green square) and quartz cement (%; black cross) versus depth. (D) Core photographs overlain with facies boundaries (white dashed lines), facies association or subfacies codes, and location of sub-samples (orange star with green rim) used for textural and composition analyses. (E) Mineral abundance measured by SEM-EDS analysis. Note that mineral percentages start at 55% to better visualise changes in phyllosilicate, pyrite and feldspar abundances. (For interpretation of the references to colour in this figure legend, the reader is referred to the Web version of this article.)

operator (Equinor) from the Smørbukk field (block 6506-12; well 6506/12-N-4H); a base interval (S1) from 5986 to 5974 m RKB, a middle interval (S2) from 5956 to 5939 m RKB, and a top interval (S3) from 5907 to 5893 m RKB). These samples all derive from the upper part of the Tilje where tidal-fluvial processes dominated (Ichaso and Dalrymple, 2014). This was a deviated well; the true vertical depths below mud line for these intervals are 4263 to 4257 m TVD, a middle interval (S2) from 4248 to 4239 m TVD), and a top interval (S3) from 4223 to 4216 m TVD. The development well 6506/12-N-4H was drilled in the year 2000 in a water depth of 272 m and was plugged in 2017. Rather than use the conventional approach of thinly spreading samples for quantitative petrographic study over an entire length of core, we have instead focussed high density sampling over three sections of sandstone that represent extremes of core analysis and basic log characteristics. We here acknowledge that the 100–300 m thick Lower Jurassic Åre and Tilje Formations represent a highly-heterogeneous succession (Dreyer, 1992; Ichaso and Dalrymple, 2009; Ichaso et al., 2016; Martinius et al., 2001, 2005). Additional studies would be required to create a predictive scheme for the entire succession across the whole basin; however, this study highlights the detailed, time-consuming, and thus expensive approach required to unravel such sedimentological and petrophysical complexity. This study involved the integration of core description, core analysis data (porosity and permeability), and high-density sampling for light microscopy and optical point-counting (sediment composition and grain size), Backscattered Scanning Electron Microscopy (BSEM), and cathodoluminescence (SEM-CL) and Scanning Electron Microscopy-Energy Dispersive Spectroscopy (SEM-EDS) data to better understand the distribution of reservoir quality in the three studied intervals.

3.1. Core description: facies associations and depositional elements

Core description (at the centimetre scale) was undertaken to define the different facies (F), subfacies (SF), and Facies Associations (FA) in each interval to better understand the primary depositional environment. Facies and subfacies were principally discriminated based on lithology, sand-mud ratio, and physical sedimentary structures, as well as the type and degree of bioturbation. The common co-occurrence of

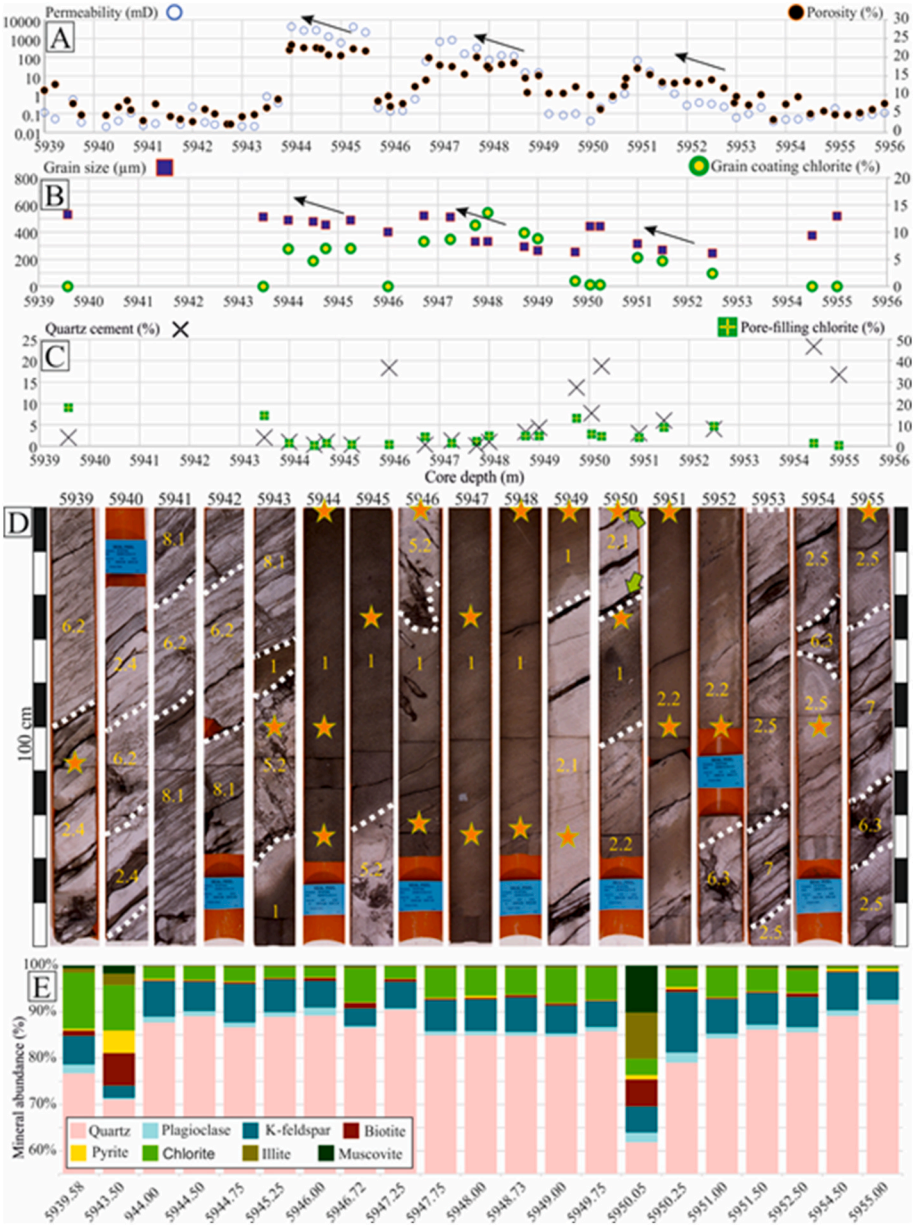

Fig. 6. Summary panel of section two (S2; middle interval, Fig. 3) from 5956 to 5939 m (measured depth), interpreted to be deposited in a tidal-fluvial channel setting. Note that this core is wholly in facies association 2. (A) Porosity (%; dark brown circles with orange rim) and permeability (mD; hollow blue circles) versus depth. Black arrows highlight cycles of increasing permeability which corresponds to an increasing sediment grain size (average; blue square with red rim) observed in panel B. (B) Grain-coating chlorite (%; yellow circles with green rim) and grain size versus depth. (C) Pore-filling chlorite (%; yellow cross in green square) and quartz cement (%; black cross) versus depth. (D) Core photographs overlain with facies boundaries (white dashed lines), facies association or subfacies codes, and location of sub-samples (orange star with green rim) used for textural and composition analyses. (E) Mineral abundance measured by SEM-EDS analysis. Note that mineral percentages start at 55% to better visualise changes in phyllosilicate, pyrite, and feldspar abundances. (For interpretation of the references to colour in this figure legend, the reader is referred to the Web version of this article.)

specific facies was used to establish facies associations (FA).

Mud content was used to differentiate heterolithics, based on Ichaso and Dalrymple (2014); (1) heterolithic sandstones (<10% mud interbeds), (2) sand-dominated heterolithics (10–40% mud interbeds), (3) mixed sand-mud heterolithics (40–60% mud interbeds), (4) mud-dominated heterolithics (60–90% mud interbeds), and (5) mudstone (>90% mud interbeds). Bed thickness was assigned based on Ingram (1954), i.e., laminae (<1 mm thick), very thin-bedded (1 mm–3 mm), thin-bedded (3 mm–1 cm), medium bedded (1 cm–3 cm), thick bedded (3 cm–10 cm), and very thick-bedded (>10 cm). Bedding styles, which includes flaser, wavy, lenticular and pin-stripe types, was described based on Reineck and Wunderlich (1968). The determination of grain size and sorting are based upon methods defined by Folk and Ward (1957) and calculated through point-counting (see light microscopy and point counting section). The degree of sediment bioturbation was classified using a bioturbation index (BI) proposed by Taylor and Goldring (1993): 0 – no bioturbation, 1 – sparse bioturbation, bedding distinct, few discrete traces and/or escape structures, 2 – low bioturbation, bedding distinct, low trace density, escape structures often common, 3 – moderate bioturbation, bedding boundaries sharp, traces discrete, overlap rare, 4 – high bioturbation, bedding boundaries indistinct, high trace density with overlap common, 5 – intense bioturbation, bedding completely disturbed (just visible), limited reworking, later burrows discrete, 6 – complete bioturbation, sediment reworking due to repeated overprinting.

3.2. Core analysis and subsampling

Conventional core analysis data for 43 m of core (172 horizontal core plugs) were made available by the operator (Equinor). Porosity and permeability were measured on all core plugs using modern industry-standard methods and corrected for confining stress. Core analysis porosity data incorporates all types of pores, and thus includes microporosity (e.g., in altered framework grains or microporous clays) which cannot be quantified by modal or SEM-EDS analyses.

Petrographic and X-ray diffraction analyses at the University of Liverpool were performed on 56 of the 172 core plugs. A previous study on chlorite grain-coat distribution by Ehrenberg (1993) in the Smørbukk

Table 1
Facies scheme for the three sedimentary intervals used in this study. Bioturbation index (BI) has been classified after Taylor and Goldring (1993): 0 – No bioturbation, 1 – Sparse bioturbation, bedding distinct, few discrete traces and/or escape structures, 2 – Low bioturbation, bedding distinct, low trace density, escape structures often common, 3 – Moderate bioturbation, bedding boundaries sharp, traces discrete, overlap rare, 4 – High bioturbation, bedding boundaries indistinct, high trace density with overlap common, 5 – Intense bioturbation, bedding completely disturbed (just visible), limited reworking, later burrows discrete, 6 – Complete bioturbation, sediment reworking due to repeated overprinting.

Facies	Subfacies	Grain size and sedimentary structures	Bioturbation type and intensity	Environmental Interpretation
Facies 1 (F1): Cross-stratified sandstone with quartz pebbles	No subfacies	Medium- to coarse-grained, moderately well-sorted sandstone with sub-rounded quartz pebbles and granules. Individual beds have erosive basal contacts, often lined by quartz pebbles and/or granules.	BI 0. Absent. Excluding top-down *Diplocraterion* burrows which originate from overlying subfacies 5.2.	**Tidal-fluvial channel bar close to tidal-limit.** Moderate to strong fluvial currents in a fluvial-tidal channel setting. The absence of trace fossils suggests a stressed high-energy environment. Top-down bioturbation from facies 5.2 (large-scale *Diplocraterion*), probably reflects times of low river flow or temporary channel avulsion.
Facies 2 (F2): Cross-stratified heterolithic sandstones	**Subfacies 2.1: Cross-stratified sandstone with fluid mud**	Medium-grained and moderately-sorted cross-stratified sandstone with homogenous fluid mud layers (<2 cm) at basal contacts. Fluid mud layers become less frequent upward (in younger deposits) and grain-size typically increases.	BI 0. Absent.	**Tidal-fluvial channel bar at or close to the central turbidity maximum.** Moderate to strong fluvial currents leading to bar migration in a relatively proximal fluvial-tidal-channel. Fluid muds are indicative of fresh- and salt-water mixing and typically form at the base of channels and/or toes of (fluvial-) tidal-bars. The absence of trace fossils suggests a stressed environment. The reduction of fluid-mud layers in younger deposits may indicate; (i) a higher position in the channel fill, (ii) a position further up the bar and hence progressively more out of the zone where the fluid muds pass through (i.e., deeper parts of the channel), and/or (iii) a progressive reduction in suspended-sediment concentrations in the water column (possibly due to seasonality driving the migration of the turbidity maximum).
	Subfacies 2.2: Cross-stratified sandstone with flasers	Medium- to coarse-grained, moderately well- to poorly-sorted, and relatively structureless sandstones, with localised isolated mud flasers, interbedded with silty-sandstone. Bed contacts can be bioturbated or erosional.	BI typically 0 to 1 (locally 3 to 4). Absent to moderate. Small-scale *Skolithos*.	**Tidal-fluvial channel point-bar.** Moderate to high energy. Isolated mud-drapes and low bioturbation intensity (small scale *Skolithos*) indicate brackish tidal-conditions. Thin beds comprised of bioturbated silty sandstones suggest periods of lower energy. Flow-reversal structures in associated subfacies 5.1 indicate a channelised environment
	Subfacies 2.3: Bioturbated cross-stratified sandstone	Medium-grained, moderately-sorted, and intensely bioturbated cross-stratified interbedded with bioturbated silty-sandstone. Basal contacts can be sharp, erosional, gradational and bioturbated. Bed thickness and grain-size typically increased upward.	BI 2 to 4. Low to high. Small-scale mixed Cruziana-*Skolithos bioturbation assemblages*.	**Distributary mouth bar.** Low to moderate energy. An increase in bioturbation type and intensity (*Cruziana-Skolithos*) and more heterolithic nature suggest that subfacies 2.3 was deposited in a relatively unconfined distributary environment with the migration of bars over subaqueous sandflats.
	Subfacies 2.4: Trough cross-stratified sandstone with fluid mud and/or conglomeratic lag	Coarse-grained and poorly-sorted trough cross-stratified sandstone. Erosional basal contacts are lined by fluid-mud (<2 cm) and quartz granules and pebbles.	BI 0. Absent	**Tidal-fluvial dunes at or close to the central turbidity maximum.** High energy tidal-fluvial channel fill with fluid muds (indicative of fresh- and saltwater mixing) formed at the toes of lunate dunes. The absence of trace fossils supports the interpretation of a high-energy stressed environment. Thick mud layers suggest a location below, or proximal to, the turbidity maximum (similar to subfacies 2.1).
	Subfacies 2.5: Speckled sandstone with fluid mud	Medium-grained and moderately-sorted cross-stratified sandstone with single and compound fluid mud layers (<2 cm). Bioturbated and fragmented mud layers (mud	BI 1 to 4. Sparse to intense. Small scale *Skolithos*.	**Fluvial-influenced tidal-channel bar.** Low to moderate energy currents in a fluvial-tidal channel setting. Fluid muds are likely to have formed at the base of channels and/or toes of (fluvial-) tidal bars, in an environment

(*continued on next page*)

Table 1 (*continued*)

Facies	Subfacies	Grain size and sedimentary structures	Bioturbation type and intensity	Environmental Interpretation
		intraclasts) give the sandstone a speckled appearance.		subject to fresh- and saltwater mixing. Intense bioturbation suggests a less restricted environment compared to subfacies 2.1 and 2.4 (possibly a lateral equivalent or deposited in a slightly more distal setting).
Facies 3 (F3): Current rippled and cross-laminated sandstone	No subfacies	Fine-grained, well- to moderately-sorted, current rippled, cross-laminated sandstone. Current-ripple laminar sets are bound by double mud drapes and flow-reversal structures.	BI 0 to 1. Absent to sparse. Small scale *Skolithos* and a single large-scale *Diplocraterion trace*	**Tidal-channel bar with slow-moving currents.** Slow to moderate tidal currents generate ripple cross-laminations. Flow reversal structures bind stacked-sets of current ripples and indicate a channelised system (singular flow path) subject to little to no fluvial or wave influence.
Facies 4 (F4): Cross-stratified sandstone with sand-mud couplets	**Subfacies 4.1: Cross-stratified sandstone with sporadic sand-mud couplets.**	Medium- to coarse-grained sandstone with an abundance of sand-mud couplets (note that grain-size was difficult to quantify due to intense stylotization at grain-contacts; especially at sand-mud couplet boundaries).	BI 0. Absent.	**Confined tidal dune.** Subfacies 4.1 and 4.2 represent the migration of tidal dunes in a tidal channel setting. Sand-mud couplets are deposited during the reversal of flow. Sand-mud couples are preferentially eroded in the top-sets of tidal dunes (subfacies 4.1), but are preferentially preserved in the toe-sets of tidal dunes (subfacies 4.2). Laminae sets of sand-mud couplets with (subfacies 4.2) becomes less frequent upward (in younger deposits) which may indicate channel shallowing leading to increased erosion.
	Subfacies 4.2: Laminae-sets of sand-mud couplets	Medium- to coarse-grained sandstone with an abundance of sand-mud couplets (note that grain-size was difficult to quantify due to intense stylotization at grain-contacts; especially at sand-mud couplet boundaries).	BI 0. Absent.	
Facies 5 (F5): Sandstones with large-scale *Diplocraterion*	**Subfacies 5.1: Cross-stratified sandstone with large-scale *Diplocraterion***	Medium- to coarse-grained, moderately- to poorly-sorted sandstone with faint to clear cross-stratification and/or current ripple cross-lamination with double mud drapes. Local iron staining is present.	BI 2 to 5. Low to intense. Small scale *Skolithos* and large-scale D*iplocraterion* and *Teichichnus*	**Tidal-channel bar margin or point-bar (periodic fluvial influence).** Large-scale diplocraterion suggest a stressed (high energy) environment. Interpreted to be deposited during a period of reduced fluvial input. Flow reversal structures (i.e., reactivation surfaces and double mud drapes) suggest an environment with a single flow-path with times of little to no wave or fluvial influence.
	Subfacies 5.2: Homogenised sandstone with large-scale Diplocraterion	Medium- to coarse-grained, moderately- to poorly-sorted sandstone with barely visibly cross-stratification, ripple cross-lamination, and local double mud drapes, due to intense bioturbation.	BI 5 to 6. Intense to completely bioturbated. Small scale *Skolithos* and large-scale D*iplocraterion* and *Teichichnus*	
Facies 6 (F6): Intensely bioturbated heterolithics	**Subfacies 6.1: Bioturbated sand-dominated heterolithics (60:40 to 90:10 sandstone: mudstone)**	Fine-grained, well- to moderately-sorted sandstone with barely visible current rippled cross-lamination due to intense bioturbation (formerly facies 3).	BI 5 to 6 (mostly 6). Intense to completely bioturbated. High-diversity. Small scale *Planolites*, *Skolithos* and less common large-scale *Diplocraterion*	**Tidal-channel bar margin or point-bar** Barely visible remnants of flow reversal structures, which bind stacked-sets of current ripples, indicate a channelised system (singular flow path) subject to negligible fluvial or wave influence. Subfacies 6.1 is an intensely bioturbated version of facies 3 and reflects a period of reduced sedimentation and colonization of the sediment substrate by a wide-range of ichnofauna.
	Subfacies 6.2: Bioturbated mixed sand/mud heterolithics (40:60 to 60:40 sandstone: mudstone)	Very fine- to medium-grained, poorly- to moderately-sorted, bioturbated sand-dominated heterolithics with locally preserved current-ripple cross-lamination, flaser and lenticular bedding.	BI 3 to 5. Moderate to intense. High diversity. *Planolites*, *Skolithos, Diplocraterion, Teichichnus, and Chondrites.*	**Subaqueous tidal-flat.** The diverse and abundant trace-fossil suite indicates shallow to mid-tier deposit-feeding and suspension-feeding communities in a low-energy subaqueous tidal flat setting. Rarely preserved ripple cross-lamination suggests slow-moving tidal currents.
	Subfacies 6.3: Bioturbated mud-dominated heterolithics (10:90 to 40:60 sandstone: mudstone)	Very fine- to fine-grained, poorly- to moderately-sorted, bioturbated mixed sand and mud heterolithics with locally preserved current-rippled cross-lamination.	BI 3 to 6. Moderate to intense. High diversity. *Planolites*, *Skolithos, Diplocraterion, Teichichnus, and Chondrites.*	
Facies 7 (F7): Wavy-bedded sand-dominated heterolithics showing current-ripple cross lamination	No subfacies	Wavy-bedded fine-grained, moderately well-sorted, sandstone with ripple cross lamination bound by homogenous and laminated mud layers (0.5–3 cm thick).	BI 0 to 1. Absent to sparse. Small scale *Skolithos* and *Diplocraterion* in sand intervals. Small scale *Planolites* in laminated and lenticular-bedded mudstone layers**.**	**Tidal-fluvial channel.** Low to moderate energy. Tidal currents generate ripple cross-laminated sets which are bound by abundant fluid mud layers to form a wavy-bedded style.
Facies 8 (F8) Lenticular-bedded ripple cross-laminated sandstone	**Subfacies 8.1 Bioturbated lenticular-bedded ripple cross-laminated sandstone**	Intensely biouturbaed very fine- to fine-grained, poorly-sorted, with locally preserved ripple cross-laminated and lenticular bedding..	BI 3 to 5. Low to high. *Skolithos*, *Diplocraterion, Planolites, Paleophycus, Cyclindrichnus* and *Chondrites.*	**Tidal-fluvial channel margin or point-bar top.** Current-rippled lenticular bedding indicates a tidal-fluvial channel margin or point-bar

(*continued on next page*)

Table 1 (*continued*)

Facies	Subfacies	Grain size and sedimentary structures	Bioturbation type and intensity	Environmental Interpretation
	Subfacies 8.2 Non-bioturbated lenticular-bedded ripple cross-laminated sandstone	Very fine- to fine-grained, poorly-sorted,sandstone with clear current-ripple cross-lamination and lenticular bedding.	BI 0	top setting. The diverse and abundant trace-fossil suite indicates shallow- to mid-tier deposit-feeding and suspension-feeding communities (subfacies 8.1). Brackish conditions and/or high rates of sediment deposition is the preferred interpretation for lenticular bedded with little to no bioturbation (subfacies 8.2)

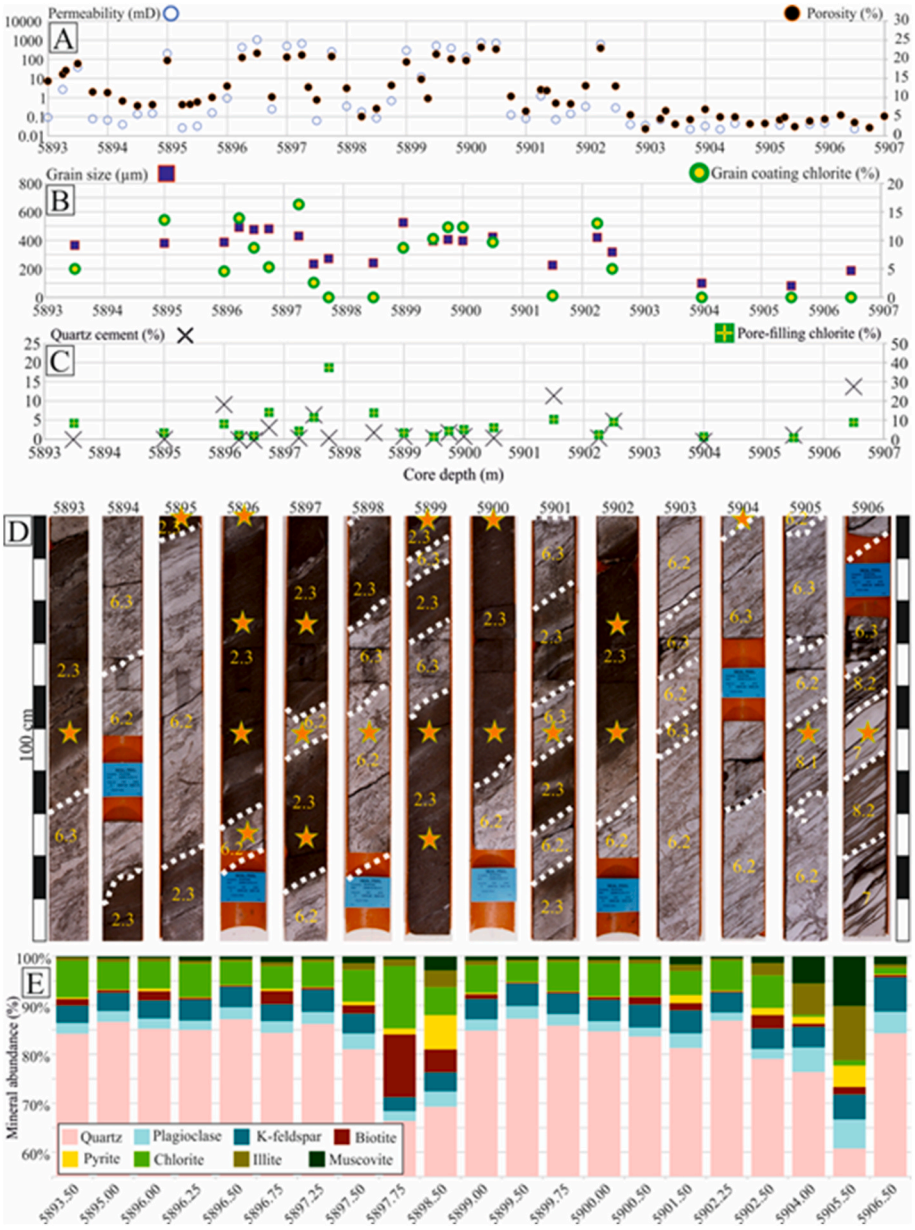

Fig. 7. Summary panel of section three (S3; top interval, Fig. 3) from 5907 to 5893 m (measured depth), interpreted to be deposited in a distributary mouth bar setting. Note that this core is wholly in facies association 3. (A) Porosity (%; dark brown circles with orange rim) and permeability (mD; hollow blue circles) versus depth. (B) Grain-coating chlorite (%; yellow circles with green rim) and grain size (average; hollow red circle) versus depth. (C) Pore-filling chlorite (%; yellow cross in green square) and quartz cement (%; black cross) versus depth. (D) Core photographs overlain with facies boundaries (white dashed lines), facies association or subfacies codes, and location of sub-samples (orange star with green rim) used for textural and composition analyses. (E) Mineral abundance measured by SEM-EDS analysis. Note that mineral percentages start at 55% to better visualise changes in phyllosilicate, pyrite and feldspar abundances. (For interpretation of the references to colour in this figure legend, the reader is referred to the Web version of this article.)

field did not include low porosity zones as it was considered that low porosity intervals were "unrelated to the problem of porosity preservation by chlorite". However, recent studies by Wooldridge et al. (2017a), Griffiths et al. (2019a), and Virolle et al. (2020) have shown the importance of understanding both the fine- and coarse-fraction with regards to understanding how precursor minerals and detrital clay-coats are distributed in the primary depositional environment. As a result, this study has assessed the mineralogical variability within both high and low net-to-gross facies, including strata bounding fluid mud.

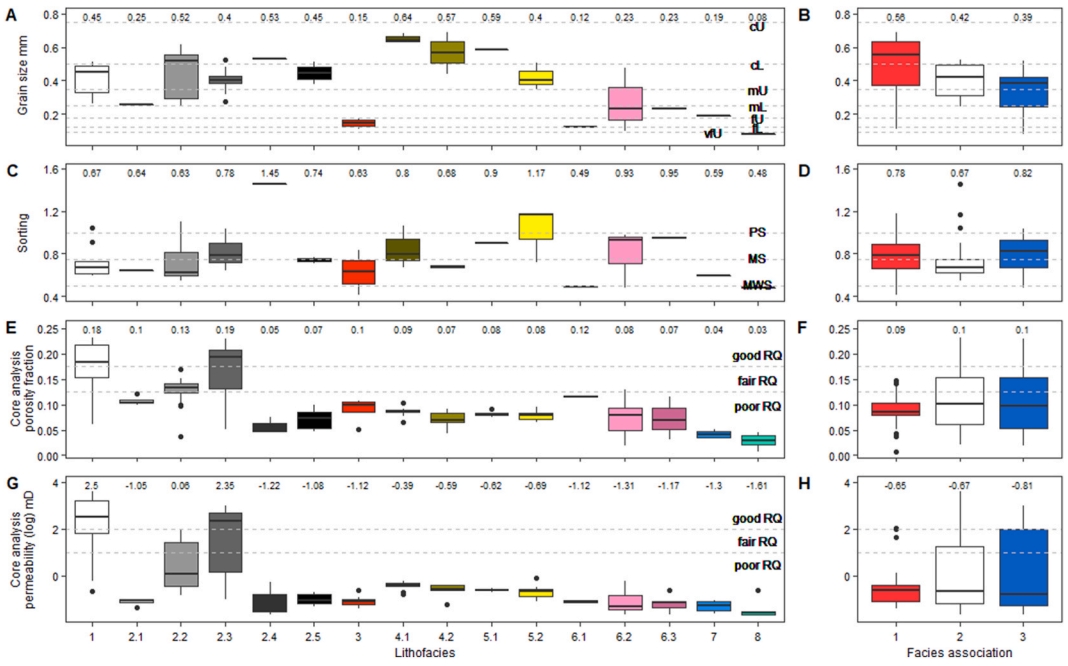

Fig. 8. Grain size, sorting, porosity and permeability as a function of the 16 different facies and subfacies and for the three facies associations. (A) Average grain-size (μm) for facies. (B) Average grain-size (μm) for facies associations. (C) Grain-size sorting (σ_1) for facies. (D) Grain-size sorting (σ_1) for facies associations. (E) Porosity (%) for facies. (F) Porosity (%) for facies associations. (G) Permeability (mD) for facies. (H) Permeability (mD) for facies associations. Measurements that are numerically distant from the rest of the data (i.e., a value that is 1.5 times the interquartile range below the lower quartile and above the upper quartile) are defined as outliers (open circles). Median values per facies and facies association are shown above each boxplot in each of Fig. 8A–G.

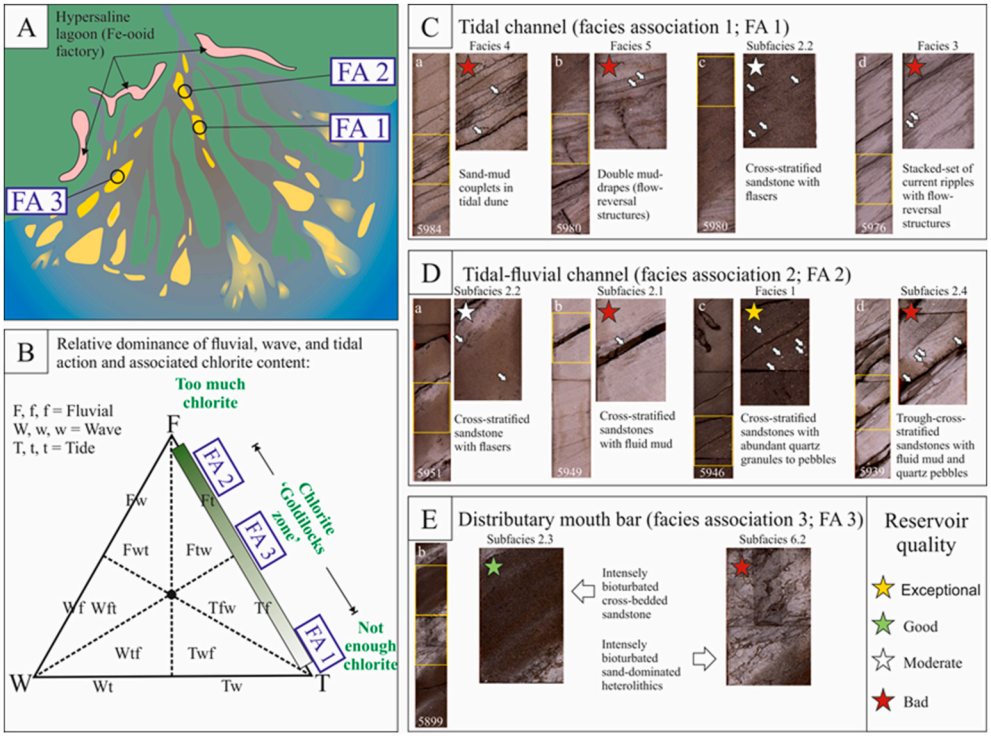

Fig. 9. Gross depositional environment and reservoir quality summary of facies associations 1, 2 and 3. (A) Interpreted gross depositional environment of facies associations 1, 2 and 3, superimposed on a modified palaeogeography from Ichaso and Dalrymple (2014). The turbidity maximum zone is approximately aligned with the area marked for FA 2. (B) Interpreted dominant coastal processes (fluvial, wave, and tidal) active during the deposition of facies associations 1, 2 and 3 using a standardised classification scheme proposed by Ainsworth et al. (2011). The abundance of chlorite associated with the relative dominance of fluvial and tidal influence is highlighted; chlorite 'Goldilocks zone' refers to sufficient quantities of chlorite to form near-continuous grain coats leading to moderate to exceptional reservoir quality. Strong tidal conditions, evidenced in FA 1, lead to a scarcity of chlorite (and so samples become quartz cemented), whereas settings that are subject to substantial (excessive) fluvial input are prone to pore-filling chlorite, as evidenced in FA 2. The optimum conditions for intermediate quantities of chlorite are mixed tidal-fluvial, as evidenced in facies 1 which is part of FA 3. (C–D) Examples of key diagnostic sedimentary structures that have led to interpreted palaeogeographic reconstructions in panels A and B. Reservoir quality, based on permeability, is highlighted for each facies by stars, where gold stars indicate exceptional reservoir quality (~100's to 1000's of mD), green stars indicate good reservoir quality (100's of mD), white stars indicate moderate reservoir quality (10's of mD), and red stars indicate bad reservoir quality (<10 mD). (For interpretation of the references to colour in this figure legend, the reader is referred to the Web version of this article.)

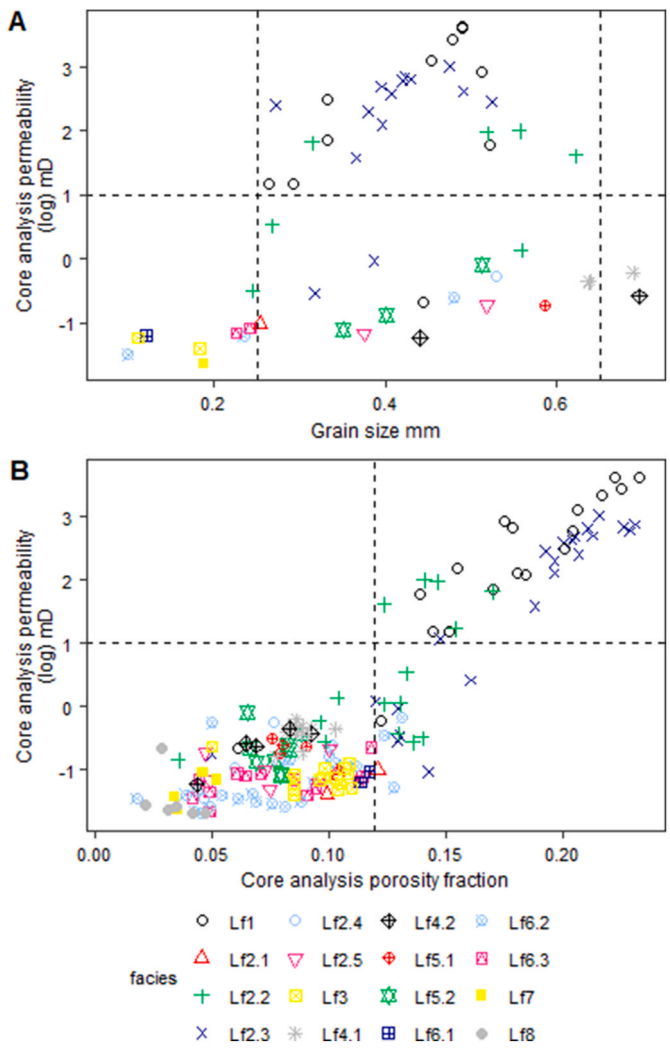

Fig. 10. Relationship between porosity, permeability, facies and grain size. (A) Permeability versus mean grain size as a function of facies. (B) Permeability versus porosity as a function of facies.

3.3. Light microscopy and optical point-counting

Light microscopy and optical point-counting (Emery and Robinson, 1993) were undertaken on polished sections made from horizontal core plugs, previously used for conventional core analysis. Point counting was undertaken to quantify grain-size (mean grain-size and sorting; through measuring the long- and short-axis of detrital grains), detrital framework-grain mineralogy, porosity (type and percentage), fine-grained matrix (type and abundance) and the mineralogy and morphology of authigenic components, e.g., grain-coating versus pore-filling chlorite. Furthermore, point-counting can distinguish between detrital quartz grains and authigenic quartz cement, as well as quantify different types of quartz grains, namely polycrystalline versus monocrystalline, which can be used to infer a change in sediment provenance (Dickinson and Suczek, 1979; Weltje, 2006). An Analysis of Variance (ANOVA) approach was used to assess whether there is a statistical difference ($p < 0.05$) in grain populations, as described by Dickinson and Suczek (1979), between each facies association.

Petrog (PETROG System, Conwy Valley Systems Ltd (CVS), UK), a statistical point-counting system with an automated stepping stage (Pantopoulos and Zelilidis, 2012; Wooldridge et al., 2017a), was used to accurately record and quantify the point count data. We here acknowledge that the reliability of modal analysis is highly dependent on the user's experience level including their ability to identify the presence of clay minerals, as opposed to oxides, organics and fine-grained carbonate minerals (e.g., siderite), and then to discern chlorite from other clay minerals such as illite and smectite. Furthermore, the spatial resolution of optical point-counting is approximately 1–5 μm (dependent on textural and mineralogical complexity) and microporosity, by definition, cannot be accounted for. In addition, studies have shown that statistical uncertainty is associated with point counting due to stereology, which may be reduced but not eliminated with an increase in the number of points counted. For example, Van der Plas and Tobi (1965) show that 10% point counted chlorite has an uncertainty of about 3.5% for 300 points counted per section, compared to around 1.8% for 1000 points counted per section. A pragmatic approach was adopted for this study; 300 points were counted for both compositional and textural analysis.

3.4. Backscattered electron microscopy (BSEM), cathodoluminescence (SEM-CL) and energy-dispersive spectroscopy (SEM-EDS)

Backscattered Electron Microscopy (BSEM) was carried out using a Hitachi TM3000 table-top SEM at an accelerating voltage of 5 or 15 kV and a working distance of 17.5 mm to capture high-resolution images of diagenetic phases.

Quantitative evaluation of minerals by scanning electron microscopy and energy-dispersive spectroscopy (SEM-EDS) was achieved using polished section in a FEI WellSite QEMSCAN. A tungsten filament produced the focused electron beam, running at 15 kV, with a sample current of 7 nA measured at the Faraday cup. During routine operation of the SEM-EDS, the system was re-calibrated for beam current and backscatter signal every time a new sample was loaded. The SEM system was programmed to collect secondary X-ray spectroscopic data across a pre-defined area of the sample using the iMeasure® software that controls the SEM-EDS. For this work, 2 μm spacing between data collection points was employed for high resolution images, e.g., capturing chlorite grain coats. In contrast, 20 μm spacing between data collection points was employed to calculate the bulk mineralogy across the entire thin section. Analysis at systematically varied step-sizes for the same sample has previously shown that the mineral quantities remain credible up to 50 μm spacing between analysis points on a grid across a sample (Pirrie et al., 2004). Once the elemental concentration has been measured at each point by the EDS detectors, the software automatically matches it with a library of mineral definitions. These mineral definitions are called SIPs (Species Identification Protocols) and are assembled in a SIP list that is effectively an archived mineral library. Each mineral is assigned a colour, and these data points are combined to form a contiguous false colour image of the sample. In addition to the images, the sum of each occurrence of an identified mineral is tabulated so that minerals and groups of minerals may be quantified.

Two energy dispersive X-ray spectrometers, produced by Bruker, recorded the discrete secondary X-rays that are emitted by the sample excited by the focused electron beam. The X-ray spectrum from each analysis point was processed to identify and quantify the elements present and output a chemical composition. The chemical composition that was recorded was matched to the SIP library of pre-defined chemical compositions for various phases including minerals, glasses and other amorphous materials. SEM-EDS does not measure or use crystallographic features and so cannot discriminate between amorphous and crystalline phases, or crystallographic polymorphs. Furthermore, SEM-EDS is also not capable of differentiating minerals with the same composition, for example rutile and anatase (TiO_2). However, SEM-EDS can be used to define similar minerals with subtle difference in composition, for example chlorite with different Fe–Mg ratios (Worden et al., 2018b).

To accurately distinguish between quartz overgrowths and detrital quartz grains in heavily-quartz cemented sandstones SEM-CL images were taken using a Philips XL30 SEM equipped with a K.E. Developments Ltd cathodoluminescence (CL) detector (D308122) by

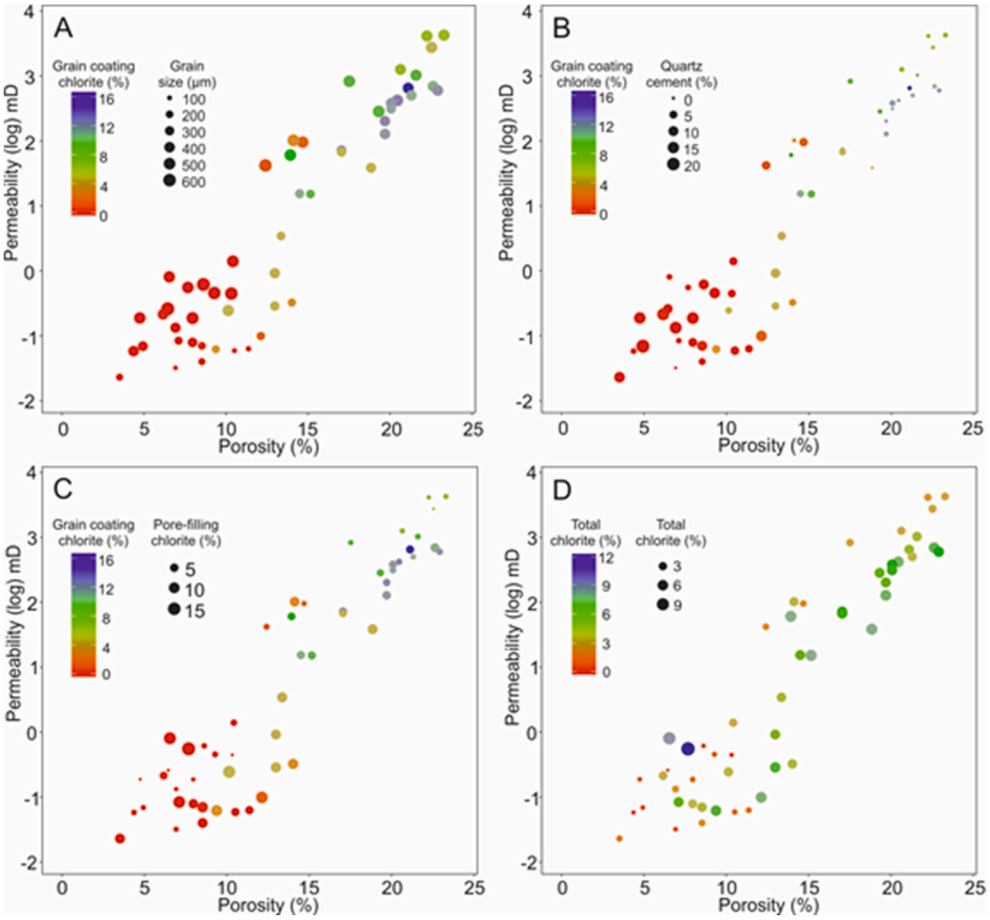

Fig. 11. Comparison of core analysis porosity and permeability plotted as a function of a variety of reservoir quality controls denoted by colour and symbol size. (A) Porosity and permeability plotted as a function of grain size (symbol size) and the volume of grain-coating chlorite (colour). (B) Porosity and permeability plotted as a function of quantity of quartz cement (symbol size) and the volume of grain-coating chlorite (colour). (C) Porosity and permeability plotted as a function of pore-filling chlorite (symbol size) and volume of grain-coating chlorite (colour). (D) Porosity and permeability plotted as a function of total chlorite (symbol size and colour. (For interpretation of the references to colour in this figure legend, the reader is referred to the Web version of this article.)

integrating the signal of 16 frames using a slow scanning raster at 10 kV and spot size 7.

4. Results

In this section, we present results from detailed core descriptions (facies scheme), conventional core analysis (porosity and permeability), light microscopy and optical point-counting, BSEM, SEM-CL and SEM-EDS analyses.

4.1. Facies and facies associations

In summary, the three studied core intervals from well 6506/12-N-4H display a great deal of heterogeneity in terms of grain size, bedding style, sedimentary structures, bed thickness, and bioturbation type and intensity, over relatively short vertical distances (typically <1 m) (Fig. 4). In total, eight facies, which divide into sixteen subfacies, and three facies associations have been identified. The interpreted facies boundaries defined in the sedimentary log (Fig. 4) can be observed on core photographs in Figs. 4–6. Table 1 provides detailed facies and subfacies descriptions and environmental interpretations, based on grain size, bedding style, sedimentary structures, bed thickness, and bioturbation type and intensity. Sediment grain size and sorting, derived from point-counting for each facies, are presented alongside core photographs (Figs. 5B, 6B and 7B), and summarised, as a function of facies and subfacies, as box and whisker plots in Fig. 8A and B.

The common co-occurrence of specific facies was used to establish the following three facies associations (FA): tidal-channel (FA 1), tidal-fluvial channel (FA 2), and distributary-mouth bar (FA 3), which broadly correlates with sections S1, S2 and S3, respectively (Fig. 9). Section 1 (Fig. 5; bottom interval) is comprised almost entirely of FA 1 and is interpreted to be the result of tidal-channel processes. Tidal-channel facies association-1 (FA 1) contains facies 2.2, 3, 4.1, 4.2, 5.1, 5.2, 6.1, 6.2 and 8.1. The interpretation of a tidal channel depositional environment (singular flow path), with little to no fluvial or wave influence, was selected due to the common occurrence of sand-mud couplets (facies 4), flow reversal structures or double mud-drapes (facies 3 and subfacies 5.2) and stacked-sets of current-rippled and cross-laminated sandstones (facies 3; Fig. 9C).

Section 2 (Fig. 6; middle interval) is comprised almost entirely of FA 2 and is interpreted to be the result of tidal-fluvial channel processes. Tidal-fluvial channel facies association-2 (FA 2) contains facies 1, 2.2, 2.4, 2.5, 6.2, 6.3, 7 and 8.1. The interpretation of a tidal-fluvial channel depositional environment (negligible wave influence) was selected due to the coarse and angular nature of the sand grains and common occurrence of quartz granules and pebbles (facies 1, and subfacies 2.4) and fluid mud layers (facies 7, 2.5, 2.1, and 2.4; Fig. 9D).

Section 3 (Fig. 7; top interval) is comprised almost entirely of FA 3 and is interpreted to be the result of unconfined distributary mouth bar processes. Distributary-mouth bar facies association-3 (FA 3) contains facies 2.3, 6.2, 6.3, 7 and 8.2. The interpretation of distributary mouth bar was made based on the overall coarsening- and thickening-upward organisation, persistent current-generated structures, and abundant tidal ichnofacies assemblages (*Cruziana* and *Skolithos*). Furthermore, unlike FA 1 and FA 2, there is a distinct lack of sand-mud couplets, double mud-drapes, or flow-reversal structures that suggests that FA 3 was not a channelised depositional environment. Similarly the absence of coarse angular sand grains or fluid mud, that would signal a high-suspended load at or close to the central turbidity maximum, suggests that FA 3 did not have a strong fluvial influence. The high net-to-gross

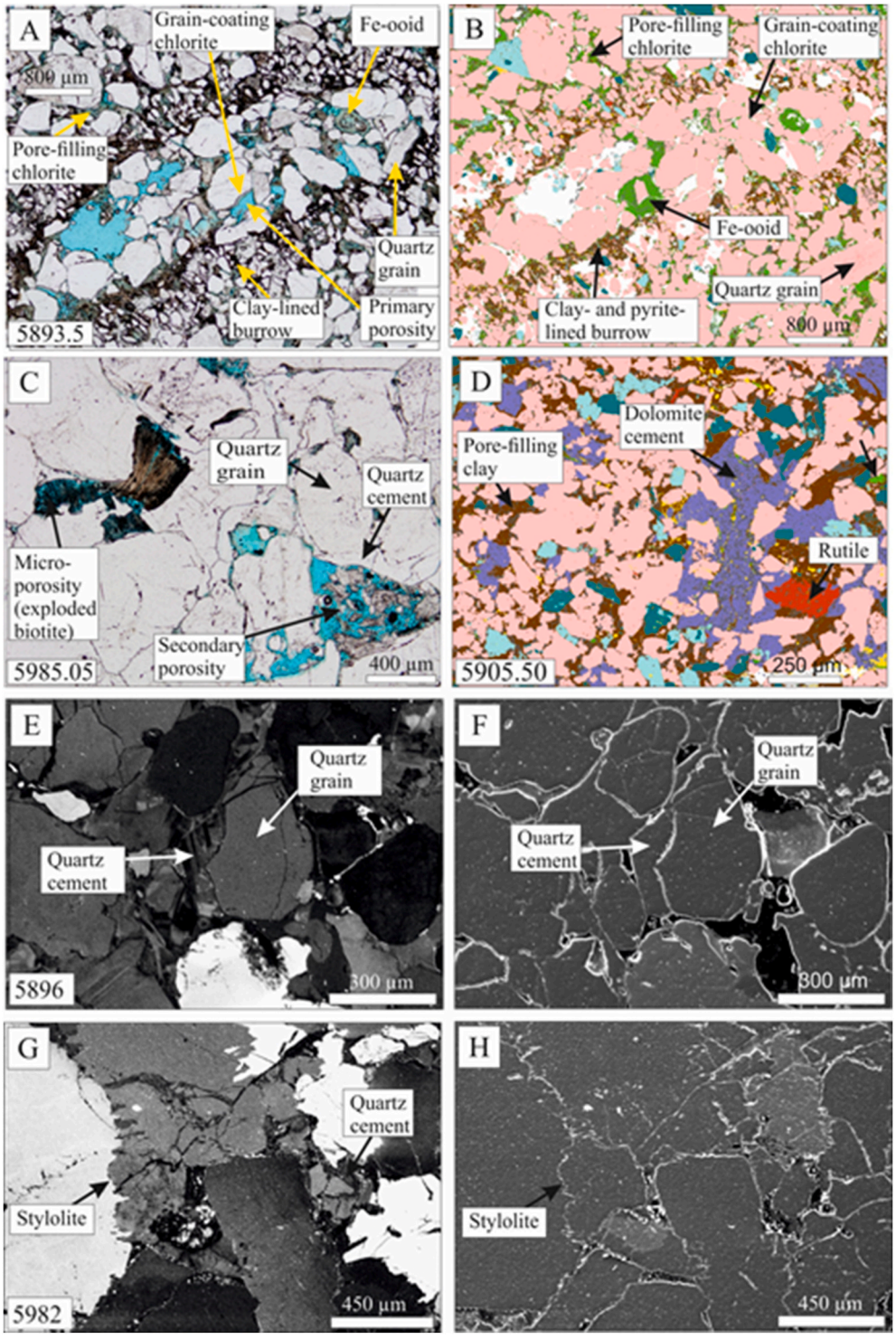

Fig. 12. Diagenetic features which impact reservoir quality to variable extents throughout the three studied sections. (A–B) Optical microscopy and SEM-EDS images of distributary mouth bar sandstone (subfacies 2.3) showing a relatively high-porosity mud-lined burrow in which chlorite-coated sand grains and Fe-ooids are situated. (C) Optical image of heavily quartz-cemented tidal-channel sandstone (subfacies 4.1) with secondary porosity due to framework grain dissolution (i.e., biotite and feldspar). (D) SEM-EDS image of a dolomite-cemented tidal-fluvial channel margin sandstone (subfacies 8.1). Dolomite cement is observed in one sample only and is not considered to have a major impact on reservoir quality in this study. (E and F) Cathodoluminescence (CL) and paired backscattered scanning electron microscopy (BSEM) images of a distributary mouth bar sandstone (subfacies 2.3) with poorly developed chlorite coats leading to authigenic quartz cementation at clean sand-grain surfaces. (G and H) CL and BSEM images of a tidal-channel sandstone showing intense stylolite-formation (exacerbated by illite and/or mica) along sand-mud couplets deposited in the toe-sets of tidal dunes (subfacies 4.2).

sections (subfacies 2.3) are interpreted to have developed from the migration of dunes and ripples over the top of the low net-to-gross sections (subfacies 6.2 and 6.3), which are interpreted as subaqueous tidal flats.

Fig. 9 provides a sedimentological summary of sections 1, 2 and 3 and highlights key palaeoenvironment indicators which has led to each facies association being positioned on a palaeogeographic reconstruction, modified after Ichaso and Dalrymple (2014). An interpretation of the dominant coastal processes (fluvial, wave, and tidal) active during the deposition of each facies association, using a classification scheme proposed by Ainsworth et al. (2011), is presented in Fig. 9B.

4.2. Porosity, permeability, texture and mineralogy

Conventional core analysis (porosity and permeability), optical point-counting (texture; grain size and sorting) and SEM-EDS (composition) data are presented in this section for each facies association. The relationships between grain size and porosity and permeability as a function of facies and percentage of grain-coating chlorite are presented in Fig. 10 and Fig. 11A–D. Analysis Of Variance (ANOVA) test results

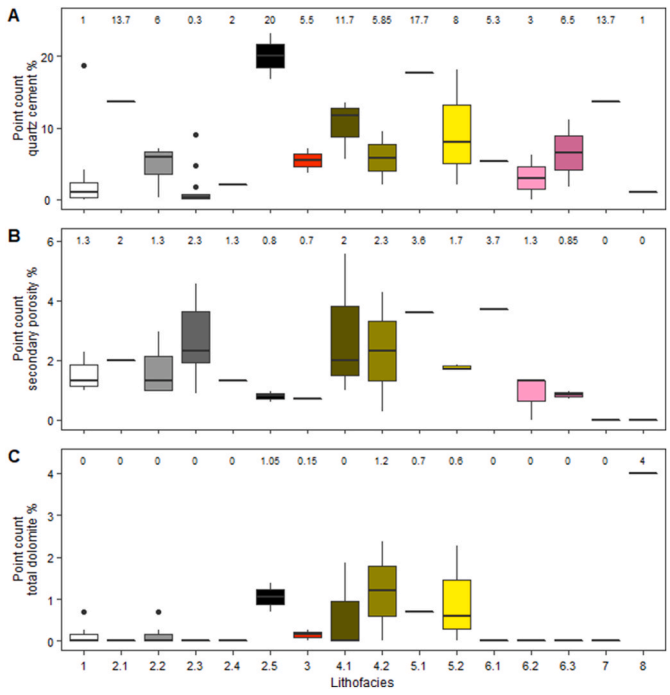

Fig. 13. Quartz cement, secondary porosity and dolomite cement as a function of the 16 different facies and subfacies. (A) Quartz, (B) Secondary porosity, (C) Dolomite. Measurements that are numerically distant from the rest of the data (i.e., a value that is 1.5 times the interquartile range below the lower quartile and above the upper quartile) are defined as outliers (open circles). Median values per facies are shown above each boxplot in each of Fig. 13A–C.

show no statistically significant difference ($p > 0.05$) in grain populations (i.e., quartz, feldspar, lithics, and the relative abundance of mono- and polycrystalline-quartz) between each facies association.

4.2.1. Tidal channel (FA 1; section 1)

Tidal-channel sandstones (facies association 1) typically have low porosity (<10%) and permeability (<10 mD) with the exception of cross-stratified sandstone with flasers (subfacies 2.2) which, in some cases, have up to ~ 15% porosity and up to 150 mD permeability (Figs. 5, 8 and 10). The grain-size and sorting for each individual facies and subfacies are presented alongside core photographs (Fig. 5B), and as box and whisker diagrams (Fig. 8A and B). It should be noted that grain-size of facies 4, derived from optical point-counting, carries a high-level of uncertainty due to intense stylolite-formation and quartz cementation.

Mineralogical variations are presented below core-photographs in Fig. 5E. Total chlorite abundance (derived from SEM-EDS) is typically between 2 and 5% throughout the succession, excluding facies 4 which has negligible chlorite (<1%). Fine-grained, current rippled and cross-laminated sandstones (facies 3) and bioturbated sand-dominated heterolithics (subfacies 6.1) are relatively phyllosilicate-rich (combined total of ~8–10%) in comparison to the rest of the coarser grained succession.

4.2.2. Tidal-fluvial channel (FA 2; section 2)

Tidal-fluvial channel sandstones (facies association 2) have highly variable porosity and permeability (Fig. 6). Cross-stratified sandstone with quartz pebbles (facies 1) has the highest porosity and permeability out of all facies (typically 15–20% porosity; 100's to 1000's of mD permeability; Fig. 6A). Tidal-fluvial channel sandstones show a stratigraphic increase in porosity and permeability, mirroring an increase in mean grain size and sorting, from approximately 5953 to 5949 m (Fig. 6A and B; Fig. 10) punctuated by subfacies 5.2 (homogenised sandstone with large-scale *Diplocraterion* which represents a hiatus in deposition). The second highest porosity and permeability in this facies association are found in cross-stratified sandstone with flasers (subfacies 2.2) which also has a slight stratigraphic increase in porosity and permeability (typically 10–15% porosity: 10's of mD permeability).

Mineralogical variations are presented below core-photographs in Fig. 6E. Total chlorite abundance (derived from SEM-EDS) is relatively uniform in FA2 (typically 2–5%) with the exception of trough-cross stratified tidal-fluvial dunes (facies 2.4; sample 5939.58) which has an abundance of chlorite (~13%).

4.2.3. Distributary mouth bar (FA 3; section 3)

Distributary mouth bar sandstone has highly variable porosity and permeability (typically 13–20% porosity; 100's of mD permeability) throughout section 3 which reflects the heterolithic nature of the bioturbated, stratified sandstone succession (subfacies 2.3). Good porosity (20–25%) and permeability (~800–1000 mD) are present, but they are highly dependent on local grain-size, sorting, clay-content and bioturbation intensity (Fig. 7).

Mineralogical variations are presented below core-photographs in Fig. 7E. Total chlorite abundance (derived from SEM-EDS) is relatively uniform (typically 5–10%), with the exception of relatively depleted chlorite abundance (<2%), and enrichment in illite and muscovite (combined total of 10–15%) in some of the finer-grained heterolithics (facies 6 and 8).

4.3. Cementation, framework-grain dissolution and bioturbation

The degree of quartz cementation of each sample is presented alongside core photographs in Figs. 5C, 6C and 7C and shown as a function of facies in Fig. 13A. In summary, quartz cementation is highly-variable throughout the three sections, however, cross-stratified sandstone with quartz pebbles (facies 1), cross-stratified sandstones with flasers (facies 2.2) and bioturbated cross stratified sandstones (facies 2.3) tend to have low quantities of syntaxial quartz overgrowths (Fig. 13A). The relationship between quartz cement and porosity and permeability as a function of percentage of grain-coating chlorite is further represented in Fig. 11B; this figure demonstrates that the highest reservoir quality sandstones (>15% porosity) are those that have negligible quartz cement and that also have an intermediate volume (5–10%) of grain-coating chlorite.

Cathodoluminescence (CL) and paired backscattered electron microscopy (BSEM) images in Fig. 12E–H provide examples of quartz cement overgrowths and intense stylolite-formation in relatively clean sandstones (typically at grain-to-grain contacts separated by muscovite/illite) in facies 4 within tidal channel sandstones (Fig. 5D). Pearson's correlation coefficient test results reveal that there is no statistically significant relationship between the relative abundance of polycrystalline quartz and abundance of quartz cement ($p > 0.05$). Dolomite cement is a minor phase in lenticular-bedded, ripple cross-laminated sandstone (facies 8) and is only found in one sample (Figs. 12D and 13C).

Secondary porosity is present in dissolved framework grains (typically feldspar and lithic fragments) and "exploded" phyllosilicates (typically biotite) (Fig. 12C). However, secondary porosity is relatively minor in all sandstones, typically being less than 3% (Fig. 13B).

The bioturbation type and intensity for each facies and subfacies are presented in Table 1. Optical microscopy and SEM-EDS images, presented in Fig. 12A and B, illustrate how early sediment bioturbation in subfacies 2.3 may have led to an increase in vertical permeability due to an abundance of mud-lined and sand-filled *Skolithos* burrows. However, intense bioturbation has also entrained fine-grained material from overlying, relatively muddy-facies (subfacies 6.2 and 6.3) into relatively clean cross-stratified sandstones (subfacies 2.3).

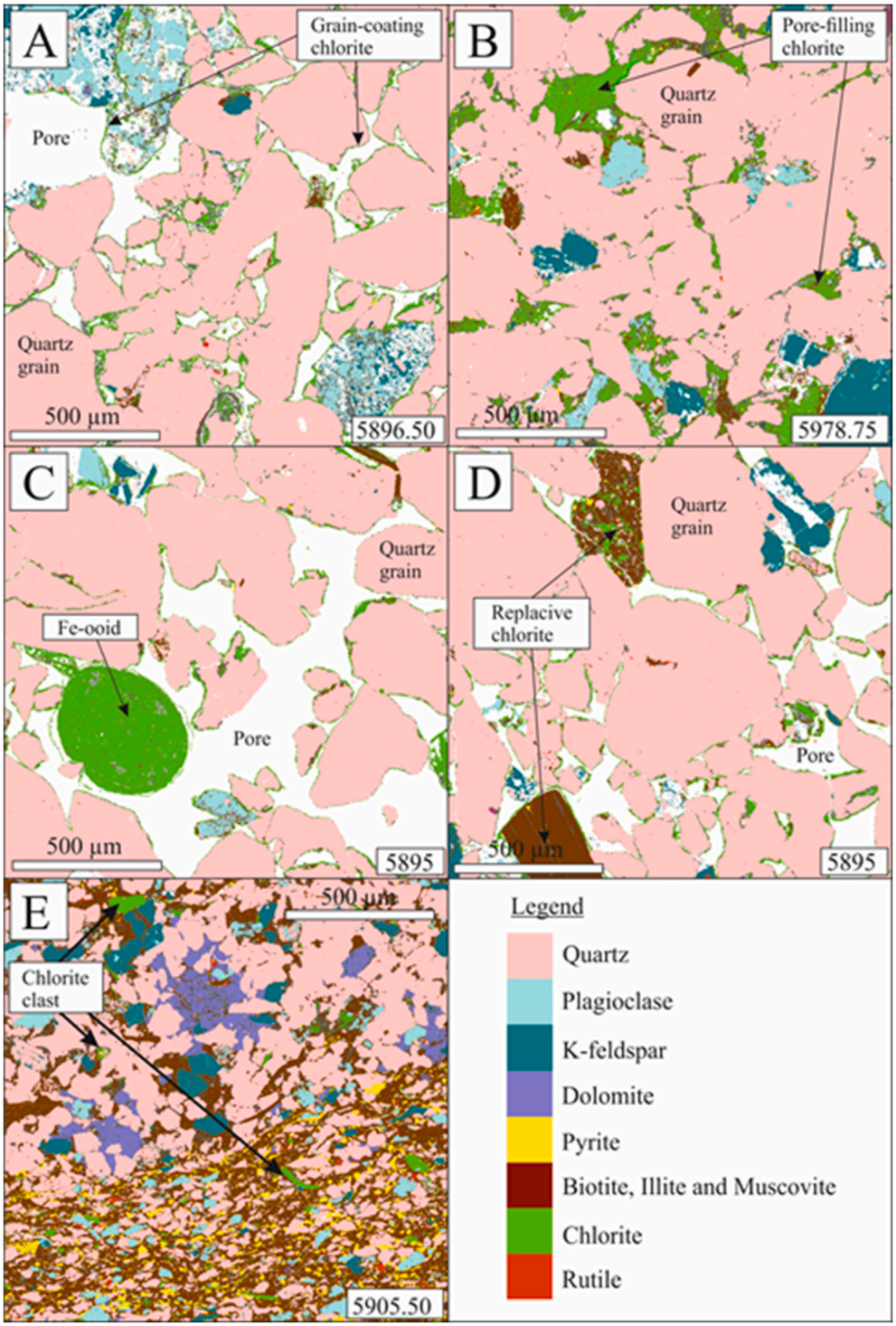

Fig. 14. SEM-EDS images showing examples of the different types of chlorite present. (A) Grain-coating chlorite in a distributary mouth bar sandstone (subfacies 2.3). (B) Pore-filling chlorite in a fine-grained tidal-channel bar sandstone deposited from slow-moving currents (facies 3). (C) Fe-ooids in a distributary mouth bar sandstone (subfacies 2.3). (D) Chlorite replacement of framework grains (principally biotite) in a distributary mouth bar sandstone (subfacies 2.3). (E) Chlorite lithics (flakes) in a tidal-fluvial channel margin heterolithics (facies 8.1).

4.4. Chlorite morphology and distribution

Six morphology classes of chlorite have been observed which are illustrated in Fig. 14. The morphological classes are as follows: (1) diagenetic grain-coating chlorite, (2) detrital grain-coating chlorite in which 10 µm flakes of detrital silt-grade chlorite are embedded (3) pore-filling chlorite, (4) chlorite-rich Fe-ooids, (5) grain-replacive chlorite, and (6) chlorite clasts (Fig. 14A–E and 15A-F). Note that we have no information about the initial mineralogy of the chlorite-rich Fe-ooids, but they are presently predominantly composed of chlorite with minor quantities of illite within the concentric layers. The presence of silt-grade chlorite in the chaotic detrital clay coats (Fig. 15b) suggests that, dissimilar to a recent example (Virolle et al., 2021), at least some of the components for diagenetic chlorite were supplied by detrital chlorite.

Grain-coating chlorite, where present, occurs on the surface of all detrital framework-grains regardless of grain mineralogy (Fig. 15). Grain-coating chlorite can be split into two phases, an inner, detrital coat in which chlorite flakes are typically subparallel to the grain surface, and an outer authigenic coat in which chlorite crystals are more fibrous and are orientated perpendicular to the grain surface (Fig. 15B). Grain-coating chlorite commonly preserves the outline of rotted K-

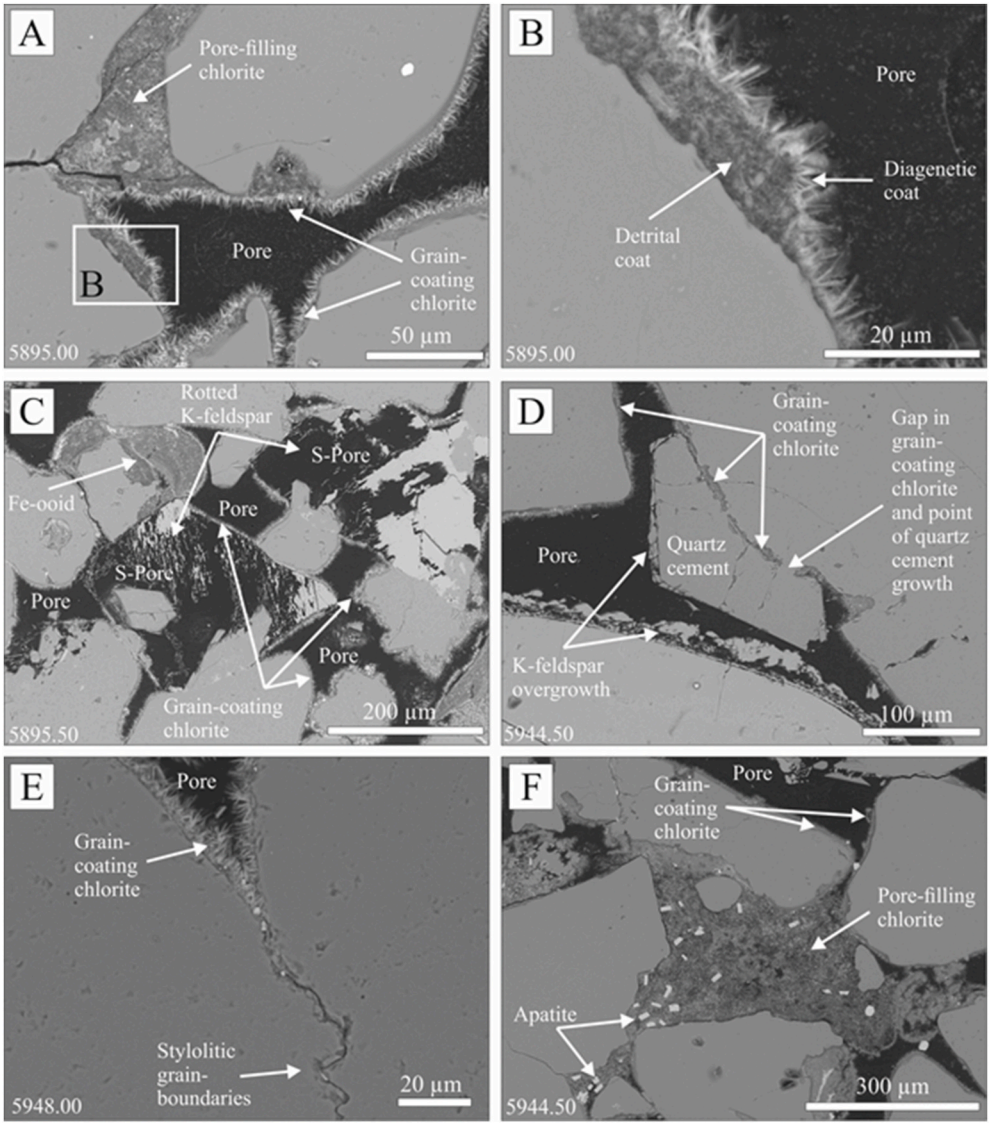

Fig. 15. Backscattered scanning electron microscopy (BSEM) images of pore-filling and grain-coating chlorite. (A) Examples of grain-coating and pore-filling chlorite in distributary mouth bar sandstone (subfacies 2.3); much detrital chlorite is preserved in grain indentations, suggesting that there may have been episodes of in-situ detrital coat creation followed by transient erosion of the initial detrital coat, except where the coat was protected in grain embayments (Verhagen et al., 2020). (B) A zoomed-in image of a chlorite coat on a sand grain surface, showing an inner detrital and outer authigenic coat. (C) Example of grain-coating chlorite covering both quartz grains and rotted K-feldspars (creating secondary porosity; labelled S-Pore) in a distributary mouth bar sandstone (subfacies 2.3). (D) Discontinuous chlorite grain coat allowing for the growth of a single syntaxial quartz overgrowth, which has later provided the surface for K-feldspar cementation, in a tidal-fluvial channel bar sandstone (facies 1). (E) Discontinuous chlorite grain coat has led to quartz grain to quartz grain contacts, forming stylolites in a tidal-fluvial channel bar sandstone (facies 1). (F) Pore-filling chlorite with an abundance of randomly distributed apatite crystals, as well as grain-coating chlorite on neighboring quartz grains in a tidal-fluvial channel bar sandstone (facies 1).

feldspar grains which have been subject to grain dissolution (Fig. 15C) but it is not seen on the surface of authigenic K-feldspar or quartz overgrowths (Fig. 15D). Breaks in chlorite grain coats, on the micrometre scale, have permitted the growth of authigenic quartz cement (Fig. 15D) and stylolite-formation (further exacerbated by the presence of illite and muscovite) (Fig. 15E).Where pore-filling chlorite is abundant (>10%), reservoir quality tends to be relatively low (porosity <15%) (Fig. 11C). It is important to note that it is the type of chlorite (grain-coating or pore-filling) that controls porosity and permeability and not the total abundance of chlorite (Fig. 11D). Pore-filling chlorite is here subdivided into five types: (a) bridging structures between sand-grains and within grain-embayments (Fig. 15A), (b) amorphous mass (Fig. 15F), (c) an abundance of detrital chlorite-flakes (Fig. 16B), (d) deformed chlorite-rich Fe-ooids (Fig. 17C–E), and (d) chloritized balls (Fig. 18).

Fe-ooids are present in most samples, but they may be classified as pore-filling chlorite where they have undergone considerable deformation, as mentioned above. Fe-ooids appeared to have nucleated on small detrital grains, such as rotted feldspars and quartz fragments (Fig. 17A and B). Authigenic chlorite grain-coats have formed on the surface of Fe-ooids after they have experienced soft-sediment deformation (Fig. 17A–F). The common occurrence of sodium chloride (NaCl; salt) is notable between the layers of chlorite ooids (Fig. 17C–F). Sodium chloride (NaCl) cannot be the product of precipitation from present-day formation waters because the formation water, with salinity values in the range of 102,000 to 118,000 ppm in the Tilje Fm in the Smørbukk field (Bybee, 2006), is highly undersaturated with respect to sodium chloride. Based on the observed textures, halite must have been present between concentric Fe-ooid layers prior to soft-sediment deformation, during early burial-compaction (Fig. 17C–F) suggesting that the halite must been present within Fe-ooids at a very early diagenetic stage. It is not easy to establish the origin of the halite, but it may imply formation of Fe-ooids in an evaporitic setting, perhaps in lagoons, on the margins of the upper part of the delta.

Minor grain-replacive chlorite is observed in most samples as a result of the alteration of Fe-rich framework grains (i.e., mafic lithics; Fig. 14D) and phyllosilicates (i.e., biotite; Figs. 14D and 16A). In intensely bioturbated sandstones, pyrite is typically observed to have grown within the burrow-network instead of chlorite (Fig. 18C).

Detrital chlorite clasts are of minor abundance in nearly all samples except in cross-stratified sandstones bound by fluid mud (facies 2.1 and 2.4; Fig. 16). SEM-EDS mineral quantification shows that fluid-mud layers are relatively chlorite-depleted and relatively illite- and muscovite-enriched (Fig. 16A).

The relative abundances of grain-coating chlorite, pore-filling chlorite, chlorite-rich Fe-ooids, grain-replacive chlorite, and chlorite clasts

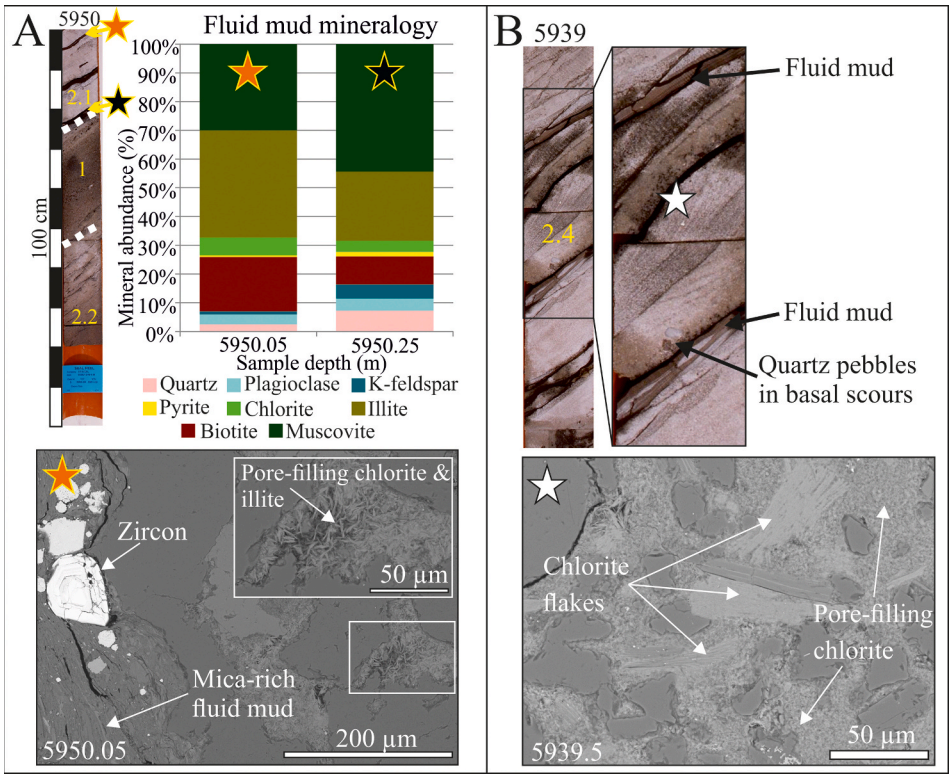

Fig. 16. Pore-filling chlorite in cross-stratified sandstones bound by fluid-mud; tidal-fluvial channel bar at, or close to, the central turbidity maximum (subfacies 2.1) and tidal-fluvial dunes at, or close to, the central turbidity maximum (subfacies 2.4). (A) Mineral abundance measured through SEM-EDS for two fluid-mud samples and backscattered scanning electron microscopy (BSEM) image (5950.05; subfacies 2.1) which captures both the mica-rich fluid-mud and overlying host-rock. A zoomed-in image of the host-rock which shows an abundance of pore-filling chlorite with minor fibrous illite (subfacies 2.1). (B) Core photograph of subfacies 2.4 and sample location of BSEM image which shows an abundance of pore-filling chlorite and detrital chlorite flakes within the foresets of trough-cross stratified sandstones bound by fluid mud layers.

are illustrated, for each section, in Fig. 19 and plotted as a function of facies in Fig. 20. In summary, tidal channel sandstones (FA 1; section 1) contains much less chlorite than tidal-fluvial channel (FA 2; section 2) and distributary mouth bar (FA 3; section 3) sandstones, and most of this chlorite in FA 1 is pore-filling as opposed to grain-coating (Fig. 19C). Chlorite is typically either grain-coating or pore-filling in tidal-fluvial channel (FA 2; section 2) and distributary mouth bar (FA 3; section 3) sandstones (Fig. 19A and B), however their distribution is heterogeneous. Grain-coating chlorite is most abundant and well-developed in cross-stratified sandstones with quartz pebbles (facies 1) in tidal-fluvial channel bars, and in bioturbated cross-stratified sandstone (subfacies 2.3) in distributary mouth bars (Fig. 20B). Pore-filling chlorite is most abundant in cross-stratified sandstones with fluid mud (facies 2.1 and 2.4) in tidal-fluvial channels (Fig. 20C).

4.5. *Timing of key diagenetic processes (paragenetic history)*

The timing of key diagenetic processes is summarised in Fig. 21, including pre-requisites to pore-filling and grain-coating chlorite. Since Fe-ooids are mechanically weak (Fig. 17E), ooid formation must have happened near to, or within, the depositional environment. Partially dissolved K-feldspar (Fig. 21) occurs as a nucleation point for Fe-ooid formation showing that K-feldspar dissolution started before deposition of the sediment (Fig. 17A). K-feldspar dissolution also occurred late in the diagenetic sequence during the formation of diagenetic chlorite coats and quartz cementation (Fig. 12C and D). Clay mineral segregation occurred in the primary sedimentary environment, as shown by the illite-rich fluidised mud and chlorite-rich sandstones (Fig. 16). Partial detrital clay coats (Fig. 15B) formed on the surface of sand grains within the primary depositional environment. It is noteworthy that early-pyrite growth seems to correlate with sediment bioturbation and the creation of mud-filled burrows. The local generation of pyrite occurred instead of Fe-clay growth due to Fe-sequestration (Fig. 18C).

The halite layers within Fe-ooids (Fig. 17) probably formed at the same time as the ooids themselves and formed prior to compaction. Since the Fe-ooids are ductile (weak), their compaction occurred relatively early so that the halite must have been present before the earliest stages of mechanical compaction. As previously discussed, K-feldspar dissolution is a continuous process and therefore secondary porosity, generated through the dissolution of K-feldspar and explosion of biotite, often postdates quartz cementation. K-feldspar overgrowths are observed on the surface of, and therefore postdate, authigenic syntaxial quartz cement overgrowths (Fig. 13D).

5. Discussion

Controls on facies distribution and compositional variation in the primary depositional environment and their implications on diagenesis and reservoir quality are discussed in this section. Attention is paid to the fundamental controls on the origin and occurrence of pore-filling and grain-coating chlorite, which are the dominant controls on reservoir quality in all three sedimentary successions.

5.1. *Deltaic facies in the Smørbukk Field: nature and organisation*

Previous regional studies (Ehrenberg et al., 1992; Ichaso and Dalrymple, 2014; Martinius et al., 2001) have shown that the synrift Tilje Formation was deposited in a relatively narrow, but long, seaway during a period of significant crustal extension during the Jurassic. The seaway connected the Boreal and Tethys Oceans (Corfield and Sharp, 2000). Results presented here (summarised in Fig. 9) concur with earlier studies which suggested that the Tilje Formation accumulated in a shallowing-upward, heterolithic deltaic setting, in which fluvial and tidal processes predominated (Ichaso and Dalrymple, 2009, 2014; Ichaso et al., 2016; Martinius et al., 2001, 2005).

Based primarily on sedimentary structures and ichnofacies, the three studied sections from well 6506/12-N-4H are interpreted to represent transition from a tidal-channel (S1; basal interval; FA 1), to a tidal-fluvial channel (S2: middle interval; FA 2), and then into a distributary mouth-bar setting (S3: top interval; FA 3). As illustrated by Ainsworth et al. (2011), the relative dominance of fluvial, tidal, and wave processes exert a strong control on the spatial and temporal changes in

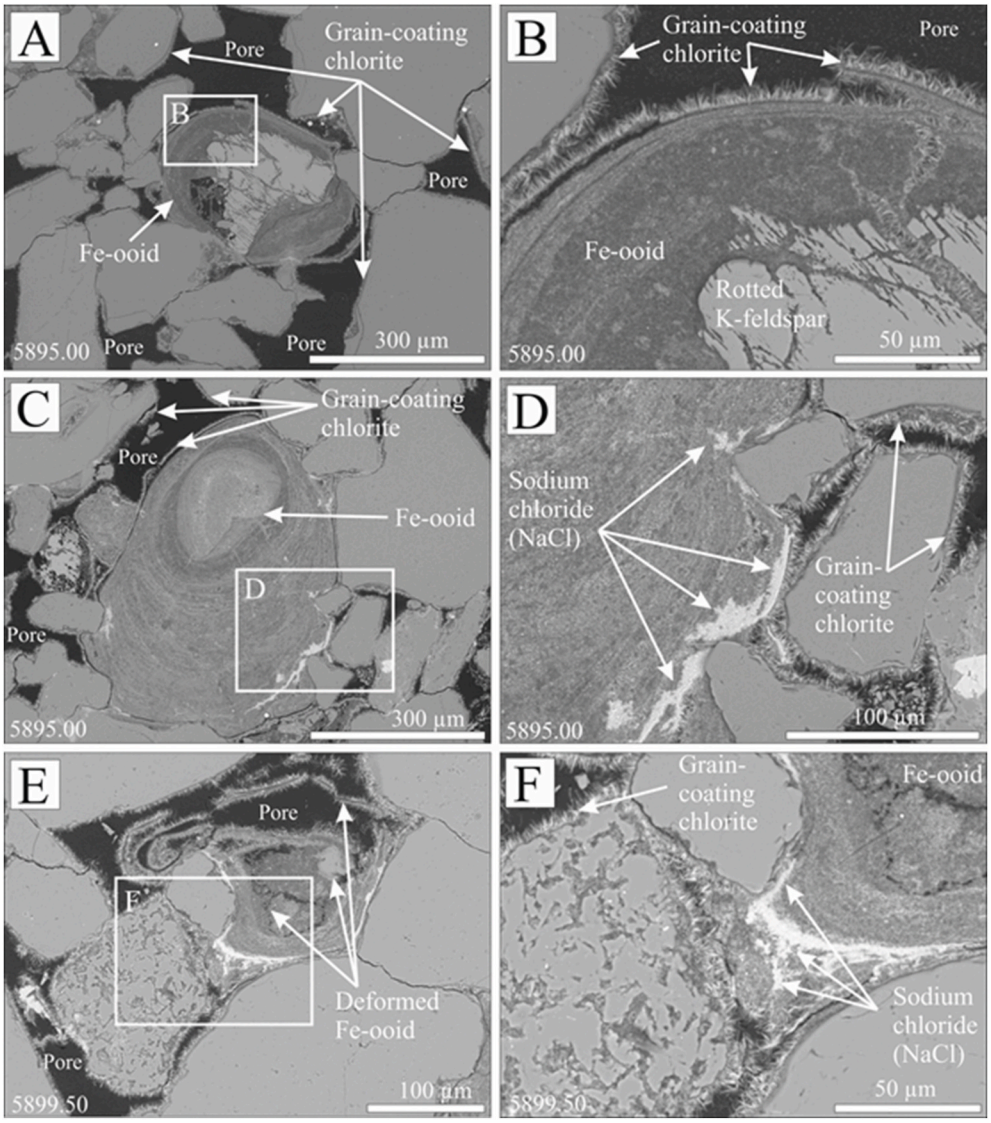

Fig. 17. Compilation of backscattered scanning electron microscopy (BSEM) images of Fe-ooids from distributary mouth bar sandstone (subfacies 2.3). (A–B) Fe-ooid (nucleated on a K-feldspar) which has deformed during compaction and then been subjected to chlorite coating. (C–F) Fe-ooids which show concentric sodium chloride (NaCl; salt) layers, which has later been deformed due to compaction, and then subject to chlorite coating. Note that, sodium chloride is not observed in the pore-space, and has also been deformed with the ooid, and is therefore likely to be a primary depositional feature.

depositional processes, and thus facies, within marginal-marine settings. Results of this study show that the distribution and abundance of grain-coating and pore-filling chlorite is strongly controlled by primary depositional processes, as reflected by the relationship between facies and reservoir quality (Figs. 8–10). For example, where fluvial influences are strong, there is a marked increase in the presence of chlorite-rich Fe-ooids and fluidised mud (Figs. 16 and 18F).

The relative decrease in the abundance of tidal indicators in facies association 2 (Fig. 6), coupled with the presence of the coarsest channel deposits and an abundance of fluid-mud, suggests that the tidal-fluvial channel deposits are the most proximal in the succession and were probably deposited at, or close to, the tidal limit (Figs. 6 and 9), in broad agreement with Ichaso and Dalrymple (2014) and Ichaso and Dalrymple (2009). The interpretation of distributary mouth bar deposits in facies association 3 (Fig. 7) is based on abundant tidal structures and moderate to intense bioturbation of mixed *Cruziana-Skolithos* ichnofacies, in agreement with the interpretation by Ichaso and Dalrymple (2014).

The transition from strictly tidal (FA 1) to tidal-fluvial deposits (FA 2) and then distributary mouth deposits (FA3) is here interpreted to be the result of longitudinal shifting of depositional environments (proximal and distal) in response to autogenic lobe switching, eustatic sea-level change and tectonically-generated accommodation space. The Tilje Formation was deposited during warm climatic conditions at a mid-palaeolatitudinal location (Ichaso and Dalrymple, 2014). However, strong seasonal differences in temperature and rainfall led to fluctuation between the two dominant processes; fluvial and tidal (Ichaso and Dalrymple, 2014). As a result, parts of the delta, typically dominated by tidal action, experienced an increased input of coarser grained sediment, and localised increases in fluid mud, chlorite-rich Fe-ooids and detrital clay (facies 1, and subfacies 2.1 and 2.4; Figs. 6D and 16).

5.2. *Fundamental controls on reservoir quality: coastal hydrodynamics and Eo- and Meso-diagenesis*

In this section, the interplay between primary depositional processes (facies), eodiagenesis and mesodiagenesis is discussed in relation to their impacts on reservoir quality. Eodiagenesis occurs at temperatures less than approximately 60–70 °C, when sediment can be influenced by surface conditions and is in the biologically active zone (Griffiths et al., 2019a; Morad et al., 2000; Worden and Morad, 2003). Mesodiagenesis occurs at temperatures greater than 70–80 °C, away from both surface conditions and the biologically active zone. One of the major processes during mesodiagenesis is kinetically-controlled quartz cementation (Worden et al., 2018a). The timing of key primary depositional and diagenetic processes (paragenetic history) is summarised in Fig. 21.

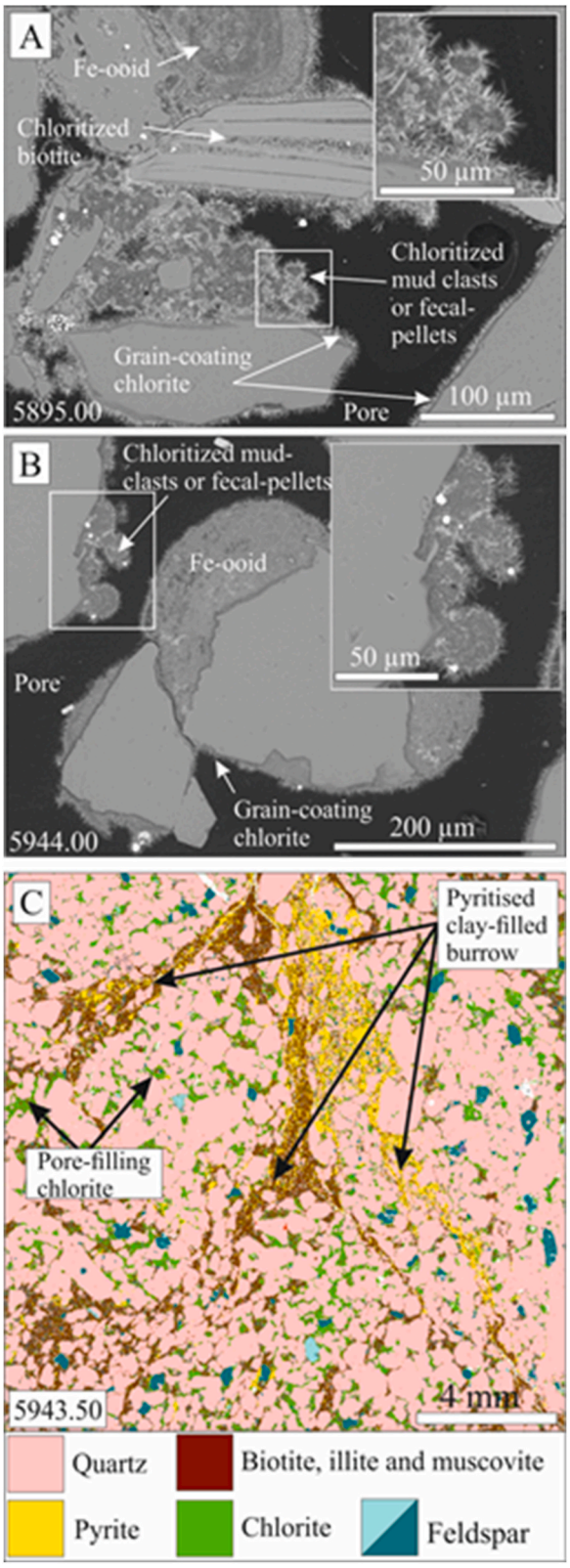

Fig. 18. Bio-sediment interaction. (A–B) Backscattered scanning electron microscopy (BSEM) images of chloritised pellets (pore-filling), interpreted to be faecal-pellets, or mud clasts, in both distributary mouth bar and tidal-fluvial channel sandstones (subfacies 2.3 and facies 1 respectively). (C) SEM-EDS image of a pyritised and biotite-rich mud-lined burrow (*Diplocraterion*) surrounded by a host-rock that has an abundance of pore-filling chlorite (tidal-channel bar margin or point-bar; subfacies 5.2).

5.2.1. Influence of coastal hydrodynamics on textural and compositional distribution patterns: implications for sandstone diagenesis and reservoir quality

Reservoir quality (porosity and permeability) of sandstone is initially governed by sediment texture (i.e., grain size and sorting) and composition (i.e., ductile versus brittle grains) (Beard and Weyl, 1973; Griffiths et al., 2019a; Scherer, 1987) (Fig. 11). During sediment transport, relatively weak framework grains (e.g., feldspars) typically reduce in size compared to more resistant grains (i.e., quartz) (Griffiths et al., 2019a; Odom et al., 1976). As a result, sediment comprised of a high abundance of weak framework grains tend to have finer-grain size and/or a wider grain-size distribution (Griffiths et al., 2019a; Odom et al., 1976). In the Tilje Formation (at least for well 6506/12-N-4H) the relationship between grain size and permeability is not simple (Figs. 9 and 11A), because of grain-coating and pore-filling chlorite (Figs. 5–7, 11B–C). However, in cross-stratified sandstones (e.g., facies 1) with chlorite grain coats which preserve porosity by inhibiting quartz cementation, permeability increases with an increase in grain size (Fig. 6A and B).

As previously discussed, sediment composition is a primary control on reservoir quality due to the relative abundance of ductile (e.g., mica) versus brittle (e.g., quartz) grains governing the extent of compaction (Aagaard et al., 2000; Ramm, 1992; Ramm and Bjorlykke, 1994). During eodiagenesis, mechanical compaction and pseudo-matrix formation is intensified by an abundance of ductile grains (Bloch, 1991; Morad et al., 2010; Ramm and Bjorlykke, 1994; Scherer, 1987; Worden et al., 2000). Sediment entry points have been reported to switch from the north toward the west during the deposition of the Tilje Formation in the Smørbukk field (Doré, 1991; Hallam, 1994; Ichaso and Dalrymple, 2014). Our analysis of variance (ANOVA) tests show broadly constant QFL proportions between the studied intervals, which possibly indicates a relatively constant drainage of broadly similar continental block lithologies (Dickinson and Suczek, 1979) and, overall, there is evidence for a relatively stable mid-palaeolatitudinal climate and generally uniform sediment provenance (Doré, 1991; Hallam, 1994; Ichaso and Dalrymple, 2014). In shallow-marine environments, mineral distribution patterns are controlled by a combination of the grain size of specific minerals and coastal hydrodynamics, and thus vary as a function of depositional environment (Griffiths et al., 2018, 2019a, 2019b; Virolle et al., 2019a, 2019b). Results of this Smørbukk study show that tidal-channel, fine-grained, current rippled and cross-laminated sandstones (facies 3) are relatively enriched in phyllosilicates (i.e., illite and muscovite; Fig. 5D) which has led to exacerbated porosity-loss during burial due to grain re-arrangement and soft-sediment deformation (Fig. 5A; Fig. 21). In contrast, coarse-grained tidal-fluvial channel dunes, deposited during periods of high riverine influx, close to the turbidity maximum (facies 2.4) are relatively enriched in pore-filling chlorite (Fig. 16). In addition to detrital chlorite flakes, coastal hydrodynamics also exert a strong control on the distribution of Fe-ooids in the Smørbukk field, leading to a concentration of Fe-ooids in relatively coarse-grained deposits (Fig. 19). Sandstones deposited in a confined tidal-channel environment away from fluvial input have a distinct lack of Fe-ooids and pore-filling and grain-coating chlorite. However, illite and muscovite are concentrated at the toe-sets of tidal dunes, in sand-mud couplets, which has led to enhanced chemical compaction (stylolite-formation) and quartz cementation (Figs. 9C and 12G). Quartz cement abundance is strongly limited by the presence of chlorite grain coats (Figs. 1, 5–71B) and thus masks any theoretical relationship between quartz cement and the abundance of polycrystalline quartz, as previously reported by Worden and Morad (2000) and Lander et al. (2008).

5.2.2. Bio-physicochemical processes and early-mineral alteration (eodiagenesis): implications for sandstone mesodiagenesis and reservoir quality

Clay minerals and clay-grade material (<2 μm in grain-diameter) can

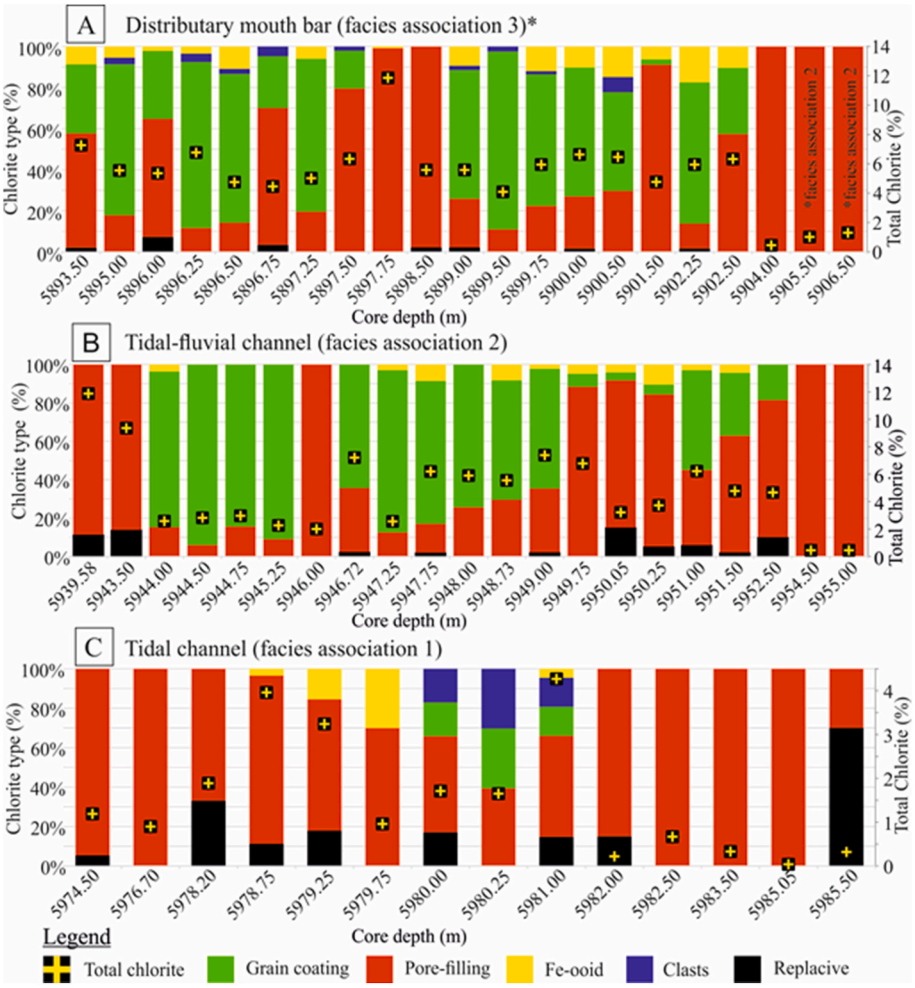

Fig. 19. Total chlorite (black square with yellow cross) and the proportions of different chlorite types, namely grain-coating (light green), pore-filling (red), clasts (blue), Fe-ooids (yellow), and replacive (black) versus measured depth. (A) Distributary mouth bar (facies association 3), excluding samples 5905.50 and 5906.50 which are facies association 2, (B) Tidal-fluvial channel (facies association 2), (C) Tidal-channel (facies association 1). (For interpretation of the references to colour in this figure legend, the reader is referred to the Web version of this article.)

be added to sediment soon after deposition due to bioturbation (Griffiths et al., 2018). Sediment bioturbation in the Tilje Formation has led to the juxtaposition of coarse- and fine-grained material from overlying- or underlying-facies (Figs. 5–7) which may alternately enhance or degrade reservoir quality. For example, very fine-grained thin-beds of subaqueous tidal-flat sandstones (subfacies 6.2 and 6.3) may benefit from the entrainment of coarse-grained sediment due to sediment bioturbation in the overlying distributary mouth bar sandstones (subfacies 2.3). Furthermore, sediment composition may be altered due to bioturbation through the direct ingestion and excretion of clay- and silt-grade material (McIlroy et al., 2003; Needham et al., 2004, 2005; Worden et al., 2006). Burrows in the Tilje Formation tend to be pyritised (Fig. 18C) which inhibits the growth of chlorite during diagenesis due to reduced Fe-availability (Griffiths et al., 2018).

5.3. *Origin and distribution of grain-coating and pore-filling chlorite: implications for sandstone diagenesis and reservoir quality*

Thick and continuous authigenic grain-coats originated from the thermally-driven recrystallisation of precursor detrital clay coats that formed in the primary depositional environment (Fig. 15B); this supports experimental evidence (Aagaard et al., 2000; Ajdukiewicz and Larese, 2012). Modern analogue studies of the Anllóns, Ravenglass and Gironde Estuaries (Dowey et al., 2017; Griffiths et al., 2018, 2019a, 2019b; Virolle et al., 2019a, 2019b, 2020; Wooldridge et al., 2017a, 2017b, 2018) show that detrital clay coats, in marginal marine sediments, are most common in fine-grained depositional environments. While fine grained facies in this study (e.g., facies 6 and 8) may host grain-coating chlorite, they have very low permeability due to an abundance of clay-grade material that blocks or narrows pore-throats (Fig. 6). As a result, a 'Goldilocks zone' scenario (Wooldridge et al., 2017b) is needed in order to achieve sufficient detrital clay coat coverage to produce continuous authigenic grain coats to inhibit quartz cement but without blocking pore throats (Figs. 9B and 11B). In the Smørbukk Field, medium-to coarse-grained, chlorite-coated tidal-fluvial channel bars (facies 1 in FA 2) and distributary mouth bars (subfacies 2.3 in FA 3) are in the 'Goldilocks zone' and have well-developed chlorite coats that inhibit quartz cement, resulting in excellent reservoir quality (Figs. 6, 9B and 11B). Tidal-fluvial channel point bars (subfacies 2.2 in FA 1) have intermediate reservoir quality as they are silty so that any chlorite coats cannot be as effective as in the cleaner related facies (facies 1). Tidal-fluvial sandstones (subfacies 2.1 and 2.4), that were deposited during periods of high fluvial influx or close to the central turbidity maximum zone (in beds associated with an abundance of fluid mud), are dominated by pore-filling chlorite (Fig. 16) suggesting that an excess of fluvial sediment leads to an ultimate excess of chlorite.

Thick grain-coats may block pore throats; however, the majority of pore-filling chlorite in this study has originated from the thermally-driven recrystallisation of Fe-rich clay precursors such as berthierine, Fe-rich lithics (Fig. 14D), chlorite clasts/flakes (Figs. 14E and 16B), and Fe-ooids (Fig. 17). Fe-ooids have been reported from a wide range of depositional environments (i.e., continental to deep marine settings) (Van Houten and Bhattacharyya, 1982; Odin, 1988) and are known to occur in the Tilje Formation (Ehrenberg, 1993). Fe-ooids have been reported to develop from a volcanic origin or weathering-derived iron solutes (Bhattacharyya and Kakimoto, 1982; Sturesson, 1994). Fe-ooids

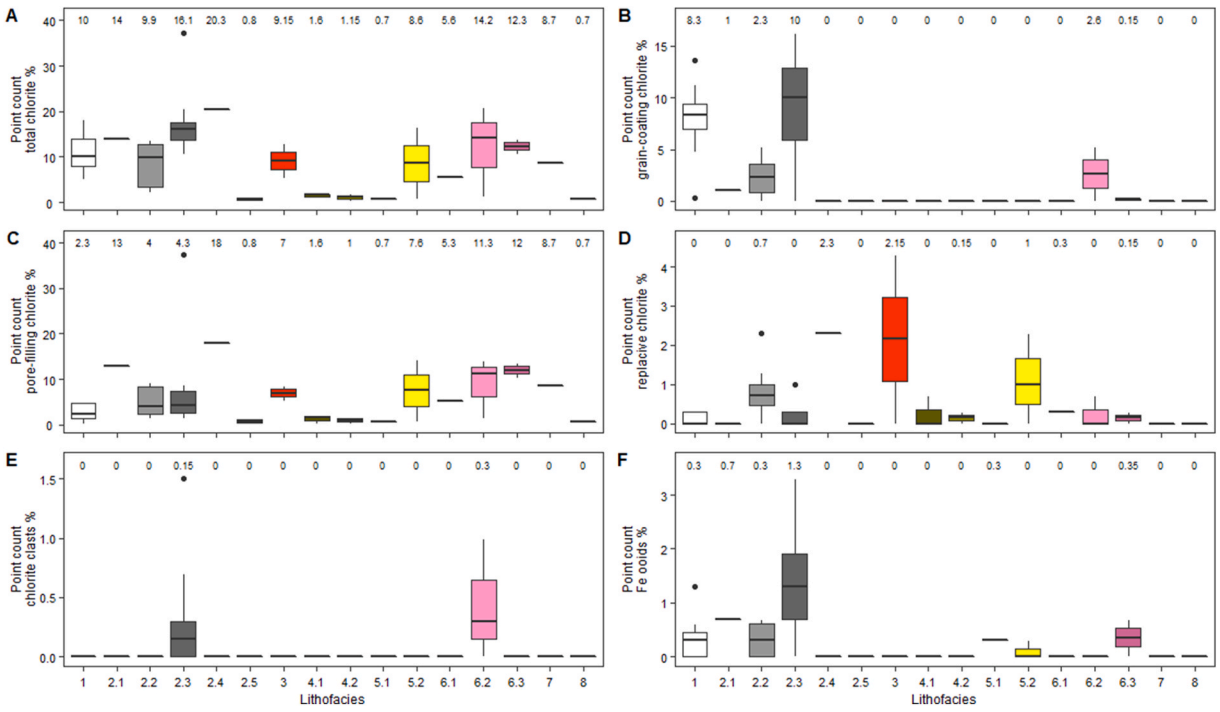

Fig. 20. The abundance of chlorite and chlorite types as a function of the 16 different facies and subfacies. (A) Total chlorite. (B) Grain-coating chlorite. (C) Pore-filling chlorite. (D) Replacive chlorite. (E) Chlorite clasts. (F) Fe-ooids (chloritised). Measurements that are numerically distant from the rest of the data (i.e., a value that is 1.5 times the interquartile range below the lower quartile and above the upper quartile) are defined as outliers (open circles). Median values per facies are shown above each boxplot in each of Fig. 20A–F.

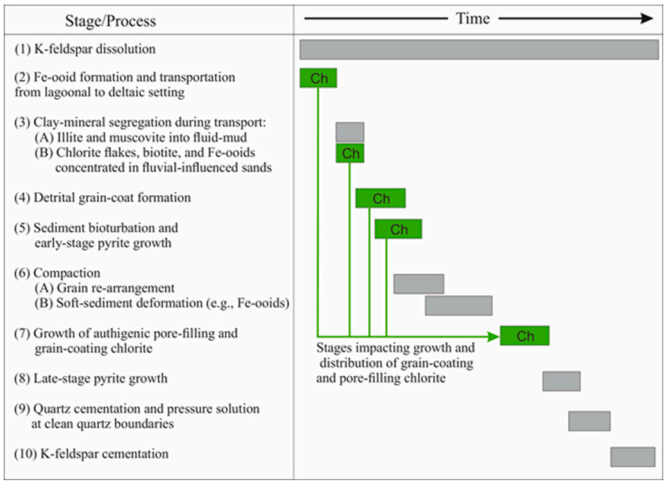

Fig. 21. Paragenetic sequence highlighting the timing of key primary depositional and diagenetic processes that have impacted reservoir quality, either directly (e.g., quartz cement) or indirectly (e.g., growth of pyrite at the expense of chlorite due to sediment bioturbation). Stages/processes that have impacted the formation and/or distribution of grain-coating and pore-filling chlorite are highlighted in green and labelled Ch. Note that, K-feldspar is a relatively unstable mineral and is subject to dissolution throughout time (e.g., it formed nucleation points for Fe-ooids in the primary depositional environment, as well as providing a source potassium for K-feldspar overgrowths during late-stage burial diagenesis). (For interpretation of the references to colour in this figure legend, the reader is referred to the Web version of this article.)

present in this study seem to have evidence of their formation in an evaporitic lagoonal-setting due to the abundance of sodium-chloride which occurs between ooid-layers (Fig. 17). Sodium-chloride has developed during the formation of ooids and has not resulted from any NaCl-saturated oil field formation brines, since both the concentric-ooid-layers and interlayered sodium-chloride have experienced early soft-sediment ductile deformation during burial (Fig. 17C–F) and the present-day formation water is highly undersaturated with respect to NaCl; salinities for the Tilje Fm. in the Smørbukk field are 102,000 to 118,000 ppm (Bybee, 2006). As a result, we here make a novel proposal that the Fe-ooids in the Tilje Formation formed in a transiently isolated evaporitic lacustrine, lagoon or tidal-flat setting and were subsequently transported throughout the delta during periods of high fluvial discharge (Fig. 9). We note that there is a paucity of known modern analogues for Fe-ooid formation but there seems to be no other process that could lead to the combination of Fe-clay accumulation and halite precipitation.

6. Conclusions

(1) In agreement with published literature on the Tilje Formation, deltaic sandstones in well 6506/12-N-4H were dominated by tidal and fluvial processes during sediment deposition. The relative dominance of tidal and fluvial processes has had a profound impact on the nature and organisation of the facies. Complex reservoir architecture associated with the three facies associations (namely, tidal channel, tidal-fluvial channel, and distributary mouth bar deposits) is here interpreted to result from switching between the relative dominance of tidal versus fluvial processes and lateral and longitudinal (proximal and distal) shifting of depositional environments. The changes probably occurred in response to seasonal variability in rainfall (possibly climatic variability), autogenic lobe switching, eustatic sea-level change and tectonic generated accommodation space.

(2) Over-and-above the well-established first-order controls on porosity and permeability (grain size, sorting, composition, detrital clay content), here the major control on sandstone reservoir quality in well 6506/12-N-4H is the presence or absence of grain-coating and pore-filling chlorite. Grain-coating chlorite has locally prevented quartz cement growth and led to

anomalously high porosity and permeability. Sandstones without chlorite grain-coats are extensively quartz cemented. Pore-filling chlorite blocks pore-throats and has significantly reduced permeability.

(3) Grain-coating chlorite originated from the thermally-driven recrystallisation of Fe-rich, detrital clay coats comprised of clay mineral precursors, such as berthierine. The growth of grain-coating chlorite has also likely resulted from a supply of Fe from precursor Fe-rich lithics (e.g., biotite) and Fe-ooids. Pore-filling chlorite principally originated from the ductile deformation of Fe-ooids, which have been squeezed into pore-throats during burial, and the breakdown of Fe-rich lithics, such as biotite, during diagenesis. An important output of this study is the identification of NaCl layers between concentric Fe-ooid layers, suggesting that Fe-ooids formed in evaporitic-lacustrine, -lagoon, or -tidal flat settings. Understanding the spatial distribution and potential drainage of such Fe-ooid factories is likely to be crucial when trying to understand the distribution of both pore-filling and grain-coating chlorite.

(4) Grain-coating chlorite is not present in tidal channel sandstones with little to no fluvial influence. Optimum grain-coating chlorite (known as the 'chlorite Goldilocks zone'), leading to excellent reservoir quality, is found in tidal-fluvial channel bars deposited during times of low suspended load (i.e., away from the central turbidity maximum and deposited during periods of normal fluvial discharge). Grain-coating chlorite is present in distributary mouth bar sandstones although primary intergranular porosity is typically reduced due to sediment bioturbation mixing interbeds of silt-prone subaqueous tidal flat sediment with sand-prone mouth bar sands. In addition, bioturbation has locally led to the growth of pyrite at the expense of chlorite due to the sequestration of Fe, which may limit the quality (extent and completeness) of chlorite grain coats. Pore-filling chlorite is found in very high concentrations in tidal-fluvial channel sands deposited under flood conditions and/or close to the central turbidity maximum due to an over-abundance of Fe-ooids and chlorite precursors (high suspended load). As a result, the presence of fluid mud provides a useful visual indicator of the likely presence of substantial pore-filling chlorite.

Declaration of competing interest

The authors declare that they have no known competing financial interests or personal relationships that could have appeared to influence the work reported in this paper.

Acknowledgments

This work was undertaken at the University of Liverpool and funded by Equinor. We thank Equinor for their financial support and altruistically permitting the publication of this research. Special thanks are offered to FEI (now ThermoFisher) for providing the SEM-EDS (QEMSCAN®), with huge gratitude expressed to Prof Alan Butcher for facilitating this provision. We thank reviewer Benjamin Brigaud for a positive and helpful review.

References

Aagaard, P., Jahren, J.S., Harstad, A.O., Nilsen, O., Ramm, M., 2000. Formation of grain-coating chlorite in sandstones. Laboratory synthesized vs. natural occurrences. Clay Miner. 35, 261–269.

Aase, N.E., Bjørkum, P.A., Nadeau, P.H., 1996. The effect of grain-coating microquartz on preservation of reservoir porosity. AAPG (Am. Assoc. Pet. Geol.) Bull. 80, 1654–1673.

Ainsworth, R.B., Vakarelov, B.K., Nanson, R.A., 2011. Dynamic spatial and temporal prediction of changes in depositional processes on clastic shorelines: toward improved subsurface uncertainty reduction and management. AAPG (Am. Assoc. Pet. Geol.) Bull. 95, 267–297.

Ajdukiewicz, J.M., Larese, R.E., 2012. How clay grain coats inhibit quartz cement and preserve porosity in deeply buried sandstones: observations and experiments. AAPG (Am. Assoc. Pet. Geol.) Bull. 96, 2091–2119.

Armitage, P.J., Worden, R.H., Faulkner, D.R., Aplin, A.C., Butcher, A.R., Iliffe, J., 2010. Diagenetic and sedimentary controls on porosity in Lower Carboniferous fine-grained lithologies, Krechba field, Algeria: a petrological study of a caprock to a carbon capture site. Mar. Petrol. Geol. 27, 1395–1410.

Beard, D.C., Weyl, P.K., 1973. Influence of texture on porosity and permeability of unconsolidated sand. AAPG (Am. Assoc. Pet. Geol.) Bull. 57, 349–369.

Beaufort, D., Rigault, C., Billon, S., Billault, V., Inoue, A., Inoue, S., Patrier, P., 2015. Chlorite and chloritization processes through mixed-layer mineral series in low temperature geological systems a - review. Clay Miner. 50, 497–523.

Bhattacharyya, D.P., Kakimoto, P.K., 1982. Origin of ferriferous ooids; an SEM study of ironstone ooids and bauxite pisoids. J. Sediment. Res. 52 (3), 849–857.

Billault, V., Beaufort, D., Baronnet, A., Lacharpagne, J.C., 2003. A nanopetrographic and textural study of grain-coating chlorites in sandstone reservoirs. Clay Miner. 38, 315–328.

Bloch, S., 1991. Empirical prediction of porosity and permeability in sandstones. AAPG (Am. Assoc. Pet. Geol.) Bull. 75, 1145–1160.

Bloch, S., Lander, R.H., Bonnell, L., 2002. Anomalously high porosity and permeability in deeply buried sandstone reservoirs: origin and predictability. Am. Assoc. Petrol. Geol. Bull. 86, 301–328.

Bybee, K., 2006. Scale cause in the smorbukk field. J. Petrol. Technol. 58, 71–73.

Corfield, S., Sharp, I., 2000. Structural style and stratigraphic architecture of fault propagation folding in extensional settings: a seismic example from the Smørbukk area, Halten Terrace, Mid-Norway. Basin Res. 12, 329–341.

Dickinson, W.R., Suczek, C.A., 1979. Plate tectonics and sandstone compositions. AAPG (Am. Assoc. Pet. Geol.) Bull. 63, 2164–2182.

Doré, A., 1991. The structural foundation and evolution of Mesozoic seaways between Europe and the Arctic. Palaeogeogr. Palaeoclimatol. Palaeoecol. 87, 441–492.

Dowey, P.J., Worden, R.H., Utley, J., Hodgson, D.M., 2017. Sedimentary controls on modern sand grain coat formation. Sediment. Geol. 353, 46–63.

Dreyer, T., 1992. Significance of tidal cyclicity for modelling of reservoir heterogeneities in the lower Jurassic Tilje Formation, mid-Norwegian shelf. Nor. Geol. Tidsskr. 72, 159–170.

Ehrenberg, S.N., 1993. Preservation of anomalously high-porosity in deeply buried sandstones by grain coating chlorite - examples from the Norwegian continental shelf. AAPG (Am. Assoc. Pet. Geol.) Bull. 77, 1260–1286.

Ehrenberg, S.N., Gjerstad, H.M., Hadler-Jacobsen, F., 1992. Smorbukk field: a gas condensate fault trap in the haltenbanken province, offshore mid-Norway: chapter 21. In: Halbouty, M.T. (Ed.), American Association of Petroleum Geologists Memoir 54: Giant Oil and Gas Fields of the Decade 1978-1988. American Association of Petroleum Geologists Tulsa, pp. 323–348.

Emery, D., Robinson, A.G., 1993. Inorganic Geochemistry: Application to Petroleum Geology. Blackwell, Oxford.

Folk, R.L., Ward, W.C., 1957. Brazos river bar. A study in the significance of grain size parameters. J. Sediment. Petrol. 27, 3–26.

Gluyas, J., Swarbrick, R., 2004. Petroleum Geoscience. Blackwell, Oxford.

Griffiths, J., Worden, R.H., Wooldridge, L.J., Utley, J.E., Duller, R.A., 2018. Detrital clay coats, clay minerals, and pyrite: a modern shallow-core analogue for ancient and deeply buried estuarine sandstones. J. Sediment. Res. 88, 1205–1237.

Griffiths, J., Worden, R.H., Wooldridge, L.J., Utley, J.E.P., Duller, R.A., 2019a. Compositional variation in modern estuarine sands: predicting major controls on sandstone reservoir quality. AAPG (Am. Assoc. Pet. Geol.) Bull. 103, 797–833.

Griffiths, J., Worden, R.H., Wooldridge, L.J., Utley, J.E.P., Duller, R.A., Edge, R.L., 2019b. Estuarine clay mineral distribution: modern analogue for ancient sandstone reservoir quality prediction. Sedimentology 66, 2011–2047.

Hallam, A., 1994. Jurassic Climates as Inferred from the Sedimentary and Fossil Record, Palaeoclimates and Their Modelling. Springer, pp. 79–88.

Heald, M.T., Anderegg, R.C., 1960. Differential cementation in the Tuscarora sandstone. J. Sediment. Res. 30, 568–577.

Hillier, S., 1994. Pore-lining chlorites in siliciclastic reservoir sandstones: electron microprobe, SEM and XRD data, and implications for their origin. Clay Miner. 29, 665–680.

Ichaso, A.A., Dalrymple, R.W., 2009. Tide-and wave-generated fluid mud deposits in the Tilje Formation (Jurassic), offshore Norway. Geology 37, 539–542.

Ichaso, A.A., Dalrymple, R.W., 2014. In: Eustatic, Tectonic and Climatic Controls on an Early Syn-Rift Mixed-Energy Delta, Tilje Formation (Early Jurassic, Smørbukk Field, Offshore mid-Norway). From Depositional Systems to Sedimentary Successions on the Norwegian Continental Margin, vol. 46. International Association of Sedimentologists, Special Publication, pp. 339–388.

Ichaso, A.A., Dalrymple, R.W., Martinius, A.W., 2016. Basin analysis and sequence stratigraphy of the synrift Tilje Formation (Lower Jurassic), Halten terrace giant oil and gas fields, offshore mid-Norway. AAPG (Am. Assoc. Pet. Geol.) Bull. 100, 1329–1375.

Ingram, R.L., 1954. Terminology for the thickness of stratification and parting units in sedimentary rocks. Geol. Soc. Am. Bull. 65, 937–938.

Karim, A., Pe-Piper, G., Piper, D.J., 2010. Controls on diagenesis of lower cretaceous reservoir sandstones in the western sable subbasin, offshore nova scotia. Sediment. Geol. 224, 65–83.

Klefstad, L., Kvarsvik, S., Ringås, J., Stene, J., Sundsby, O., 2005. Characterization of deeply buried heterolithic tidal reservoirs in the Smørbukk Field using inverted post-stack seismic acoustic impedance. Petrol. Geosci. 11, 47–56.

Lander, R.H., Larese, R.E., Bonnell, L.M., 2008. Toward more accurate quartz cement models: the importance of euhedral versus noneuhedral growth rates. AAPG (Am. Assoc. Pet. Geol.) Bull. 92, 1537–1563.

Marsh, N., Imber, J., Holdsworth, R., Brockbank, P., Ringrose, P., 2010. The structural evolution of the Halten Terrace, offshore Mid-Norway: extensional fault growth and strain localisation in a multi-layer brittle–ductile system. Basin Res. 22, 195–214.
Martinius, A.W., Kaas, I., Naess, A., Helgesen, G., Kjaerefjord, J.M., 2001. Sedimentology of the heterolithic and tide-dominated Tilje Formation. In: Martinsen, O.J., Dreyer, T. (Eds.), Proceedings of the Norwegian Petroleum Society Conference Volume 10: Sedimentary Environments Offshore Norway — Palaeozoic to Recent. Norwegian Petroleum Society, Oslo, pp. 103–144.
Martinius, A.W., Ringrose, P.S., Brostrom, C., Elfenbein, C., Naess, A., Ringas, J.E., 2005. Reservoir challenges of heterolithic tidal sandstone reservoirs in the Halten Terrace, mid-Norway. Petrol. Geosci. 11, 3–16.
McIlroy, D., Worden, R.H., Needham, S.J., 2003. Faeces, clay minerals and reservoir potential. J. Geol. Soc. 160, 489–493.
Morad, S., Al-Ramadan, K., Ketzer, J.M., De Ros, L.F., 2010. The impact of diagenesis on the heterogeneity of sandstone reservoirs: a review of the role of depositional facies and sequence stratigraphy. AAPG (Am. Assoc. Pet. Geol.) Bull. 94, 1267–1309.
Morad, S., Ketzer, J.M., De Ros, L.F., 2000. Spatial and temporal distribution of diagenetic alterations in siliciclastic rocks: implications for mass transfer in sedimentary basins. Sedimentology 47, 95–120.
Needham, S.J., Worden, R.H., McIlroy, D., 2004. Animal-sediment interactions: the effect of ingestion and excretion by worms on mineralogy. Biogeosciences 1, 113–121.
Needham, S.J., Worden, R.H., McIlroy, D., 2005. Experimental production of clay rims by macrobiotic sediment ingestion and excretion processes. J. Sediment. Res. 75, 1028–1037.
Odin, G.S., 1988. Green Marine Clays. Oolitic Ironstone Facies, Verdine Facies, Glaucony Facies and Celadonite-Bearing Facies — A Comparative Study. (Developments in Sedimentology, 45). Elsevier, Amsterdam, pp. 1–455.
Odom, I.E., Doe, T.W., Dott, R.H., 1976. Nature of feldspar-grain size relations in some quartz-rich sandstones. J. Sediment. Res. 46, 862–870.
Pantopoulos, G., Zelilidis, A., 2012. Petrographic and geochemical characteristics of Paleogene turbidite deposits in the southern Aegean (Karpathos Island, SE Greece): implications for provenance and tectonic setting. Chemie der Erde-Geochemistry 72, 153–166.
Pirrie, D., Butcher, A.R., Power, M.R., Gottlieb, P., Miller, G.L., 2004. Rapid quantitative mineral and phase analysis using automated scanning electron microscopy (QemSCAN): potential applications in forensic geoscience. In: Pye, K., Croft, D.J. (Eds.), Forensic Geoscience: Principles, Techniques and Applications. Geological Society, Bath, pp. 123–136.
Pittman, E.D., Lumsden, D.N., 1968. Relationship between chlorite coatings on quartz grains and porosity, Spiro Sand, Oklahoma. J. Sediment. Res. 38, 668–670.
Ramm, M., 1992. Porosity depth trends in reservoir sandstones - theoretical models related to Jurassic sandstones offshore Norway. Mar. Petrol. Geol. 9, 553–567.
Ramm, M., Bjorlykke, K., 1994. Porosity depth trends in Norwegain reservoirs - assessing the quantitative effects of varying pore-pressure, temperature history and mineralogy, Norwegian shelf data. Clay Miner. 29, 475–490.
Reineck, H.-E., Wunderlich, F., 1968. Classification and origin of flaser and lenticular bedding. Sedimentology 11, 99–104.
Rider, M., Kennedy, M.J., 2011. The Geological Interpretation of Well Logs. Rider-French Consulting, Cambridge, UK.
Saïag, J., Brigaud, B., Portier, E., Desaubliaux, G., Bucherie, A., Miska, S., Pagel, M., 2016. Sedimentological control on the diagenesis and reservoir quality of tidal sandstones of the upper cape hay formation (permian, Bonaparte basin, Australia). Mar. Petrol. Geol. 77, 597–624.
Scherer, M., 1987. Parameters influencing porosity in sandstones - a model for sandstone porosity prediction. AAPG (Am. Assoc. Pet. Geol.) Bull. 71, 485–491.
Southey, R., 1837. The story of the three bears. Doctor 4.
Stricker, S., Jones, S.J., 2016. Enhanced porosity preservation by pore fluid overpressure and chlorite grain coatings in the Triassic Skagerrak, Central Graben, North Sea, UK. Geological Society, London, Special Publications 435, SP435, 434.
Sturesson, U, 1994. Iron ooids in the Lower Ordovician Huk Formation, Mjosa district, Norway. J. Geol. Soc. Sweden 116, 249–253. https://doi.org/10.1080/11035899409546190.
Taylor, A.M., Goldring, R., 1993. Description and analysis of bioturbation and ichnofabrics. J. Geol. Soc. London 150, 141–148.
Van der Plas, L., Tobi, A.C., 1965. A chart for judging the reliability of point counting results. Am. J. Sci. 263, 87–90.
Van Houten, F.B., Bhattacharyya, D.P., 1982. Phanerozoic oolitic ironstones–geologic records and facies model. Ann. Rev. Earth Planet. Sci. 10, 441–457.
Verhagen, I.T.E., Crisostomo-Figueroa, A., Utley, J.E.P., Worden, R.H., 2020. Abrasion of detrital grain-coating clays during sediment transport: implications for diagenetic clay coats. Sediment. Geol. 403, 105653.
Virolle, M., Brigaud, B., Beaufort, D., Patrier, P., Abdelrahman, E., Thomas, H., Portier, E., Samson, Y., Bourillot, R., Féniès, H., 2021. Authigenic Berthierine and Incipient Chloritization in Shallowly Buried Sandstone Reservoirs: Key Role of the Source-To-Sink Context. GSA Bulletin in press.
Virolle, M., Brigaud, B., Bourillot, R., Fenies, H., Portier, E., Duteil, T., Nouet, J., Patrier, P., Beaufort, D., 2019a. Detrital clay grain coats in estuarine clastic deposits: origin and spatial distribution within a modern sedimentary system, the Gironde Estuary (south-west France). Sedimentology 66, 859–894.
Virolle, M., Brigaud, B., Luby, S., Portier, E., Feines, H., Bourillot, R., Patrier, P., Beaufort, D., 2019b. Influence of sedimentation and detrital clay grain coats on chloritized sandstone reservoir qualities: insights from comparisons between ancient tidal heterolithic sandstones and a modern estuarine system. Mar. Petrol. Geol. 107, 163–184.
Virolle, M., Fenies, H., Brigaud, B., Bourillot, R., Portier, E., Patrier, P., Beaufort, D., Jalon-Rojas, I., Derriennic, H., Miska, S., 2020. Facies associations, detrital clay grain coats and mineralogical characterization of the Gironde estuary tidal bars: a modern analogue for deeply buried estuarine sandstone reservoirs. Mar. Petrol. Geol. 114, 104225.
Weltje, G.J., 2006. In: Ternary Sandstone Composition and Provenance: an Evaluation of the 'Dickinson Model', vol. 264. Geological Society, London, Special Publications, pp. 79–99.
Wooldridge, L.J., Worden, R.H., Griffiths, J., Thompson, A., Chung, P., 2017a. Biofilm origin of clay-coated sand grains. Geology 45, 875–878.
Wooldridge, L.J., Worden, R.H., Griffiths, J., Utley, J.E.P., 2017b. Clay-coated sand grains in petroleum reservoirs: understanding their distribution via a modern analogue. J. Sediment. Res. 87, 338–352.
Wooldridge, L.J., Worden, R.H., Griffiths, J., Utley, J.E.P., Thompson, A., 2018. The origin of clay-coated sand grains and sediment heterogeneity in tidal flats. Sediment. Geol. 373, 1910, 1209.
Worden, R.H., Armitage, P.J., Butcher, A., Churchill, J., Csoma, A., Hollis, C., Lander, R. H., Omma, J., 2018a. Petroleum reservoir quality prediction: overview and contrasting approaches from sandstone and carbonate communities. In: Armitage, P. J., Butcher, A., Churchill, J., Csoma, A., Hollis, C., Lander, R.H., Omma, J., Worden, R.H. (Eds.), Reservoir Quality of Clastic and Carbonate Rocks: Analysis, Modelling and Prediction. Special Publication. Geological Society, London, pp. 1–31.
Worden, R.H., Bukar, M., Shell, P., 2018b. The effect of oil emplacement on quartz cementation in a deeply buried sandstone reservoir. AAPG (Am. Assoc. Pet. Geol.) Bull. 102, 49–75.
Worden, R.H., Burley, S.D., 2003. Sandstone diagenesis: the evolution from sand to stone. In: Sandstone Diagenesis, Recent and Ancient, vol. 4. International Association of Sedimentologists Reprint Series, pp. 3–44.
Worden, R.H., Griffiths, J., Wooldridge, L.J., Utley, J.E.P., Lawan, A.Y., Muhammed, D. D., Simon, N., Armitage, P.J., 2020. Chlorite in sandstones. Earth Sci. Rev. 204, 103105.
Worden, R.H., Mayall, M., Evans, I.J., 2000. The effect of ductile-lithic sand grains and quartz cement on porosity and permeability in Oligocene and lower Miocene clastics, South China Sea: prediction of reservoir quality. AAPG (Am. Assoc. Pet. Geol.) Bull. 84, 345–359.
Worden, R.H., Morad, S., 2000. Quartz cementation in sandstones: a review of the key controversies. In: Worden, R.H. (Ed.), Quartz Cementation in Sandstones. Special Publication of the International Association of Sedimentologists. Blackwells, Oxford, pp. 1–20.
Worden, R.H., Morad, S., 2003. Clay minerals in sandstones: controls on formation, distribution and evolution. In: Worden, R.H., Morad, S. (Eds.), Clay Mineral Cements in Sandstones, vol. 34. International Association of Sedimentologists, Special Publications, pp. 3–41.
Worden, R.H., Needham, S.J., Cuadros, J., 2006. The worm gut; a natural clay mineral factory and a possible cause of diagenetic grain coats in sandstones. J. Geochem. Explor. 89, 428–431.
Zhu, S., Wang, X., Qin, Y., Jia, Y., Zhu, X., Zhang, J., Hu, Y., 2017. Occurrence and origin of pore-lining chlorite and its effectiveness on preserving porosity in sandstone of the middle Yanchang Formation in the southwest Ordos Basin. Appl. Clay Sci. 148, 25–38.